Rice

RESEARCH Open Access

The Histidine-25-Arginine Mutation in the Rice MACPF Protein OsCAD1 Induces Cell Death and Activates Defense Responses in the Lesion Mimic Mutant *spl17*

Dongsheng Tian[1†], Yanchang Luo[1†], Shuye Jiang[1], Yuejing Gui[1], Raji Mohan[1], Ignatius Ren Kai Phang[1], In-Cheol Jang[1,2] and Zhongchao Yin[1,2*]

Abstract

Plants defend themselves against pathogens through pattern-triggered immunity (PTI) and effector-triggered immunity (ETI), with the latter often inducing a hypersensitive response (HR) characterized by localized programmed cell death (PCD). Lesion mimic mutants (LMMs), which spontaneously form HR-like lesions in the absence of pathogen infection, have served as valuable genetic resources for dissecting the molecular mechanisms underlying cell death and immune signaling in plants. In this study, we characterize the rice lesion mimic mutant *spl17*, derived from the IR64 cultivar, and identify the mutation responsible for its phenotype. We demonstrate that the *spl17* mutation leads to the accumulation of reactive oxygen species (ROS), induces light-dependent cell death and lesion formation, elevates levels of salicylic acid (SA) and jasmonic acid (JA), activates defense-related genes, and confers enhanced resistance to *Xanthomonas oryzae* pv. *oryzae*. Using map-based cloning, we identified a single Histidine-25-Arginine substitution (*OsCAD1*^{H25R}) in *OsCAD1*, a gene encoding a membrane attack complex/perforin (MACPF) domain-containing protein in rice, as the causal mutation. CRISPR/Cas9 genome editing revealed that a knockout of *OsCAD1* (*OsCAD1*^{KO}) results in seedling lethality, whereas a weak allele (*OsCAD1*^{D8}) leads to a viable lesion mimic phenotype and enhances resistance to *X. oryzae* pv. *oryzae*. Subcellular localization studies demonstrated that eGFP-OsCAD1 is broadly distributed in *Nicotiana benthamiana* cells. Transcriptome analyses, including RNA-Seq and Gene Set Enrichment Analysis (GSEA), indicate that differentially expressed genes (DEGs) in *spl17* are enriched in catalytic activity, metabolic processes, and membrane functions. Together, these results suggest that *OsCAD1* is indispensable for rice growth and development, and that its mutation triggers cell death and defense responses.

Keywords Rice, Lesion mimic mutant, *spl17*, OsCAD1, Cell death

[†]Dongsheng Tian and Yanchang Luo contributed equally to this work.

*Correspondence:
Zhongchao Yin
yinzc@tll.org.sg

[1]Temasek Life Sciences Laboratory, National University of Singapore, 1 Research Link, Singapore 117604, Republic of Singapore
[2]Department of Biological Sciences, National University of Singapore, 14 Science Drive, Singapore 117543, Republic of Singapore

Introduction

Plants utilize pattern recognition receptors (PRRs) located on their plasma membranes to detect pathogen infections through the recognition of pathogen-associated molecular patterns (PAMPs) (Bigeard et al. 2015). This surveillance mechanism, known as pattern-triggered immunity (PTI), constitutes the first line of the plant defense system, initiating basal defense responses against a broad range of pathogens. To circumvent PTI, many pathogens secrete protein effectors that are translocated into host cells, where they interfere with host immune components, ultimately resulting in effector-triggered susceptibility (ETS). In response, plants have evolved intracellular resistance (R) proteins that recognize these effectors either directly or indirectly via effector-induced modifications of host targets (Cui et al. 2015). This recognition mechanism, termed effector-triggered immunity (ETI), is often accompanied by a hypersensitive response (HR), a localized form of programmed cell death (PCD) that serves to restrict pathogen spread by sacrificing infected cells (Balint-Kurti 2019). In general, PTI provides a rapid yet moderate level of broad-spectrum resistance, while ETI elicits a slower but more robust and pathogen-specific immune response. Lesion mimic mutants (LMMs) are genetic mutants that spontaneously develop necrotic or chlorotic lesions in the absence of pathogen infection, resembling symptoms typically caused by pathogens (Bruggeman et al. 2015). Some LMMs exhibit constitutive activation of immune responses and enhanced resistance to diverse pathogens (Lorrain et al. 2003). These mutants are frequently characterized by dysregulated PCD, elevated reactive oxygen species (ROS) accumulation, upregulation of defense-related gene expression, enhanced disease resistance, and defects in growth and development. Due to these features, LMMs have been widely used as genetic tools to dissect the molecular pathways involved in cell death and immune signaling in plants (Lorrain et al. 2003).

Members of the membrane attack complex/perforin (MACPF) superfamily play crucial roles in innate and adaptive immunity in vertebrates by forming membrane pores upon oligomerization (Lukoyanova et al. 2016). For example, perforin, a key component of cytotoxic granules in $CD8^+$ T lymphocytes (CTLs) and natural killer (NK) cells, contributes to immune defense by generating membrane pores in infected or cancerous target cells (Stepp et al. 1999; Cron et al. 2023). These pores facilitate the entry of granzymes, a class of serine proteases that activate apoptosis pathways, ultimately leading to PCD (Alexandersson et al. 2004). Interestingly, plant genomes also harbor MACPF-encoding genes (Yu et al. 2020). In *Arabidopsis thaliana*, four MACPF proteins have been identified, among which AtCAD1 (also known as AtNSL2), AtNSL1 and AtMACP2 have been implicated in plant immunity (Morita-Yamamuro et al. 2005; Noutoshi et al. 2006; Tsutsui et al. 2006; Asada et al. 2011; Fukunaga et al. 2017; Chen et al. 2020; Zhang et al. 2022a, b). Knockout mutants of *AtCAD1* (e.g., *cad1-1*, *cad1-2*, *cad1-3* and *cad1-4*) and *AtNSL1* (e.g., *nsl1-1* and *nsl1-2*) display spontaneous HR-like cell death, stunted growth, seedling lethality, elevated salicylic acid (SA) levels, and constitutive activation of defense pathways (Morita-Yamamuro et al. 2005; Noutoshi et al. 2006; Holmes et al. 2021). In contrast, mutants with weak *AtCAD1* alleles (*cad1-5*/*cad1*^{C34Y} and *cad1*^{S205F}) and *AtCAD1* RNA interference (RNAi) lines exhibit milder phenotypes (Asada et al. 2011; Holmes et al. 2021). Notably, the *cad1*^{S205F} mutant shows signs of microbial dysbiosis, suggesting a potential role for *AtCAD1* in maintaining the endophytic microbial diversity in the phyllosphere (Chen et al. 2020). While *AtCAD1* and *AtNSL1* function as negative regulators of cell death in wild-type plants and promote cell death when mutated, *AtMACP2* exhibits an inverse role by promoting cell death when overexpressed and suppressing it in knockout backgrounds (Zhang et al. 2022a, b). The PCD phenotype of *cad1-1* is largely suppressed in SA-deficient plants expressing the salicylate hydroxylase gene *NahG*, indicating that SA is essential for the onset of PCD in *cad1-1* (Morita-Yamamuro et al. 2005). However, the expression of *AtCAD1* is inducible by benzothiadiazole (BTH, a SA analog) and chitin oligosaccharides, and this induction persists in both *npr1-1*, an SA signaling mutant, and *NahG* plants (Tsutsui et al. 2006). These observations suggest that *AtCAD1*-mediated immunity is also regulated through SA-independent signaling pathways. In the context of ETI, the EDS1 protein forms functional heterodimers with either SAG101 or PAD4 to regulate downstream signaling mediated by TIR-NLR (TNL) proteins (Lapin et al. 2019). Although the *pad4-1* mutation does not fully suppress the PCD phenotype of the null mutant *cad1-1* (Tsutsui et al. 2008), the dwarfism and PCD phenotype of the weak mutant *cad1-5* are completely suppressed by *eds1-2*, implicating an EDS1-dependent TNL pathway in *cad1-5*-mediated autoimmunity (Holmes et al. 2021). Proteomic analyses have localized AtCAD1 to the plasma membrane (Alexandersson et al. 2004; De Michele et al. 2009; Elmore et al. 2012), and GFP-fusion imaging further confirmed its dual localization to both the cytosol and plasma membrane (Holmes et al. 2021). In contrast, AtNSL1 is restricted to the plasma membrane (Fukunaga et al. 2017).

Rice (*Oryza sativa*), a staple food crop for nearly half of the global population, also serves as an important model for studying immunity in monocotyledonous species. To date, approximately 30 LMM genes have been cloned in rice, revealing substantial structural and functional diversity and highlighting the complexity of lesion mimic formation pathways (Zhang et al. 2022a, b; Hou et al. 2024).

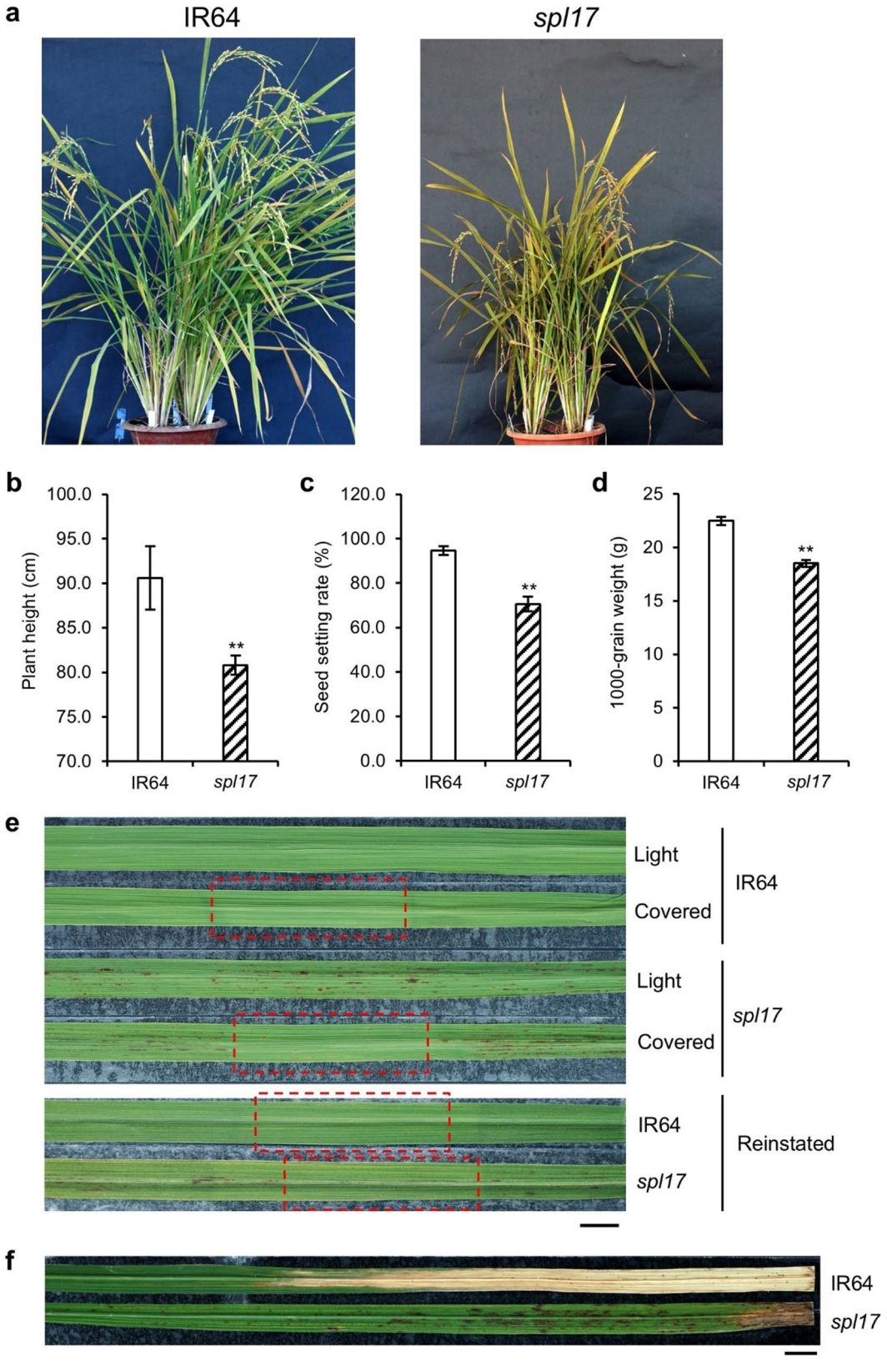

Fig. 1 (See legend on next page.)

(See figure on previous page.)

Fig. 1 Morphological and disease-related phenotypes of IR64 and *spl17*.**a** Morphological phenotypes of IR64 and *spl17* at the seed-setting stage. **b–d** Quantitative comparisons of plant height (**b**), seed-setting ratio (**c**), and 1000-grain weight (**d**) between IR64 and *spl17*. Asterisks indicate statistically significant differences ($p < 0.01$) as determined by Student's *t*-test. **e** Leaf phenotypes of IR64 and *spl17* under shading treatment. Fully expanded leaves were subjected to either natural light or shaded conditions for 7 days, followed by recovery under normal conditions for 14 days. Shaded regions are indicated by boxes. Scale bar = 1 cm. **f** Bacterial blight symptoms on IR64 and *spl17* leaves Leaves were photographed two weeks after inoculation with *X. oryzae* pv. *oryzae* strain PXO99^{A}. At least twenty leaves from four individual plants were inoculated per experiment. The experiment was repeated three times with similar results. Representative data are shown. Scale bar = 1 cm

Wu et al. (2008) described 21 *spotted leaf* (*spl*) mutants in the IR64 background, generated through mutagenesis using diepoxybutane (DEB), gamma irradiation, and fast neutron treatment. Among these, *spl17* is a recessive DEB-induced LMM that exhibits broad-spectrum resistance to *Magnaporthe oryzae*, the causal agent of rice blast, and *Xanthomonas oryzae* pv. *oryzae*, which causes bacterial blight. The *spl17* mutant also displays elevated expression of defense-related genes (Wu et al. 2008). However, the gene underlying the *spl17* phenotype has not yet been identified or characterized at the molecular level. In this study, we report the molecular cloning of *spl17* through map-based approaches, validate its function through genetic complementation and CRISPR/Cas9-mediated editing, and perform RNA sequencing to compare global gene expression profiles between IR64 and the *spl17* mutant.

Results

The *spl17* Mutation Induces Light-Dependent Spontaneous Lesion Formation and Confers Enhanced Disease Resistance in Rice

The *spl17* mutant developed dark brown spots or streaks on fully expanded leaves, beginning at the four-week-old seedling stage and persisting through the reproductive stage (Figs. 1a and 2a). Lesions initially appeared at the tips of newly emerged leaves and gradually spread across the entire leaf surface. In addition to lesion formation, the *spl17* mutation adversely affected plant growth, development, and reproduction. Compared to the wild-type cultivar IR64, *spl17* plants exhibited reduced plant height, a lower seed-setting ratio, and decreased 1000-grain weight (Fig. 1b and d). To determine whether light is required for lesion formation in *spl17*, newly emerged leaves of *spl17* plants were partially covered with aluminum foil, and lesion development was assessed seven days later. No lesions were observed in the shaded areas, whereas lesions formed in the exposed regions of the same leaves (Fig. 1e). Upon removal of the aluminum foil, lesion development resumed in the previously shaded areas (Fig. 1e). These observations demonstrate that lesion formation in *spl17* is dependent on light. To examine whether the *spl17* mutation confers enhanced disease resistance, IR64 and *spl17* plants were inoculated with *X. oryzae* pv. *oryzae* strain PXO99^{A}. The *spl17* plants exhibited enhanced resistance to PXO99^{A}, whereas IR64 plants were fully susceptible (Fig. 1f). This result is consistent with the findings reported by Wu et al. (2008).

The *spl17* Mutation Triggers Cell Death, Promotes the Accumulation of Reactive Oxygen Species (ROS), Activates the Expression of Defense-Related Genes, and Elevates Endogenous Levels of Salicylic Acid (SA) and Jasmonic Acid (JA)/Jasmonoyl-Isoleucine (JA-Ile)

Lesion formation in lesion mimic mutants is typically associated with programmed cell death, ROS accumulation, constitutive activation of defense-related genes, and alterations in plant hormone concentrations (Yin et al. 2000; Morita-Yamamuro et al. 2005; Ruan et al. 2024). To assess cell death in *spl17*, trypan blue (TB) staining, which selectively stains dead cells, was employed. Dark blue staining was observed surrounding lesions on *spl17* leaves, whereas no staining was detected in IR64 leaves (Fig. 2b). Hydrogen peroxide (H_2O_2) accumulation, a hallmark of ROS production, was evaluated using 3,3'-diaminobenzidine (DAB) staining. Lesions on *spl17* leaves exhibited intense brown staining with DAB, while IR64 leaves showed only background staining (Fig. 2c), confirming increased ROS accumulation and consequent cell death in *spl17*.

Quantitative RT-PCR (qRT-PCR) analysis revealed significant upregulation of pathogenesis-related (PR) and defense-associated genes in *spl17* compared to IR64 (Fig. 2d; Table S1). Notably, the PR genes *PR1a*, *PR2*, *PR10*, and *PBZ1* were markedly upregulated (Fig. 2d). Similarly, salicylic acid (SA) biosynthesis genes *PAL1* and *PAL2*, along with the SA signaling gene *EDS1*, exhibited elevated expression levels in *spl17* (Fig. 2d). In contrast, SA signaling genes *NPR1* and *PAD4* were either only weakly upregulated or expressed at levels comparable to IR64 (Fig. 2d). The jasmonic acid (JA) biosynthesis genes *AOS2* and *LOX*, the JA signaling genes *JAZ3* and *JAZ8*, and the JA-dependent defense-related gene *PDF1.2* exhibited either modest upregulation or expression levels comparable to those observed in IR64 (Fig. 2d). However, the JA signaling gene *JAmyb* was significantly upregulated in *spl17* (Fig. 2d). These results indicate that the *spl17* mutation strongly activates the SA-dependent pathway, while only mildly inducing the JA-dependent pathway.

Endogenous levels of SA, JA, and jasmonoyl-isoleucine (JA-Ile, the bioactive form of JA) were quantified by LC-MS/MS in four-week-old IR64 and *spl17* plants.

The SA content in *spl17* (2.1 ± 0.4 μg/g fresh weight [FW]) was 1.7-fold higher than in IR64 (1.3 ± 0.1 μg/g FW) (Fig. 2e). JA levels in *spl17* (224.5 ± 6.0 ng/g FW) were 17.1-fold higher than in IR64 (13.1 ± 1.4 ng/g FW) (Fig. 2f). Similarly, JA-Ile levels in *spl17* (22.4 ± 1.0 ng/g FW) were 71.6-fold higher than in IR64 (0.3 ± 0.1 ng/g FW) (Fig. 2g). These results indicate that both SA and JA/JA-Ile levels are significantly elevated in *spl17*, with a particularly pronounced increase in JA and JA-Ile.

The *spl17* Gene Encodes a Mutated Form of OsCAD1, Which Belongs to the Membrane Attack Complex/Perforin (MACPF) Domain-Containing Protein Family in Rice

Initial genetic mapping using an F_2 population and simple sequence repeat (SSR) markers localized the *spl17* locus to the long arm of chromosome 1 (1 L), co-segregating with the marker RM8096 (Fig. 3a; Table S2). Subsequent fine mapping with an F_3 population narrowed the candidate region to a 51-kb interval flanked by markers RMC362 (0.09 cM) and RM8096 (0.05 cM) (Fig. 3a). Whole-genome sequencing of *spl17* and IR64 identified a single A-to-G nucleotide substitution in *Os01g0748900*, which encodes a membrane attack complex/perforin (MACPF) domain-containing protein homologous to *AtCAD1* in *A. thaliana*. This gene was therefore designated *OsCAD1*. The point mutation results in a histidine-to-arginine substitution at position 25 in the spl17 variant of the protein ($OsCAD1^{H25R}$) (Fig. 3b).

Functional complementation with a 6.9-kb genomic fragment of *OsCAD1* from IR64 successfully restored the wild-type phenotype in *spl17* plants (Fig. 3c), confirming *OsCAD1* as the gene responsible for the *spl17* phenotype. Quantitative RT-PCR (qRT-PCR) analysis revealed constitutive expression of *OsCAD1* across tissues, with the highest transcript levels observed in leaves (Fig. 3d). Notably, the expression of the mutant $OsCAD1^{H25R}$ allele in *spl17* was significantly reduced compared to the wild-type allele in IR64 at all developmental stages examined (Fig. 3e).

The rice *OsCAD1* protein comprises 553 amino acid residues and contains a MACPF domain spanning positions 110 to 296 (Fig. S1). It shares 60.7% identity (336/553 residues) and 74.7% similarity (417/553 residues) with *AtCAD1* at the amino acid level (Fig. S1). Seven MACPF domain-containing genes have been identified in the rice genome: *Os01g0748900* (*OsCAD1*), *Os01g0958700*, *Os02g0475300*, *Os02g0736300*, *Os05g0557400*, *Os06g0251100*, and *Os07g0166100* (Fig. S2a), all of which encode proteins with conserved MACPF domains (Fig. S3). Phylogenetic analysis revealed that *OsCAD1* exhibits the highest frequency of amino acid substitutions per 100 residues among MACPF proteins in rice (Fig. S2b). This high level of sequence polymorphism, combined with its relatively low evolutionary conservation, suggests that *OsCAD1* may have limited or no functional redundancy with its paralogs.

Complete Loss-of-Function Mutations in *OsCAD1* are Lethal, while Hypomorphic Alleles Cause Lesion Mimic Phenotypes and Enhance Disease Resistance

To further validate *OsCAD1* as the wild-type candidate gene for *spl17*, genome editing was employed to generate knockout or knockdown mutant alleles. Two independent *OsCAD1* mutant alleles, $OsCAD1^{KO}$ and $OsCAD1^{D8}$, were generated in the genetic background of the rice cultivar Nipponbare via CRISPR/Cas9-mediated genome editing (Fig. 4a and b). In $OsCAD1^{KO}$, a 4-bp deletion (–GGGC) in exon 2 caused a frameshift mutation, resulting in a premature stop codon and the synthesis of a truncated, non-functional OsCAD1 protein consisting of 144 amino acids (Fig. 4a and b). Homozygous $OsCAD1^{KO}$ plants exhibited extensive leaf cell death and died at the seedling stage (Fig. 4c), demonstrating that OsCAD1 is indispensable for rice growth and development. Conversely, the $OsCAD1^{D8}$ mutant harbors a 24-bp deletion (–AAGGCGGGCTTGCTGGAAACAAC A) in exon 2, leading to the loss of eight amino acid residues (–KAGLLETT) at positions 99–106, located three residues upstream of the MACPF domain (Fig. 4a and b). Similar to the *spl17* mutant, $OsCAD1^{D8}$ displays a lesion mimic phenotype but remains viable, completing its life cycle and producing seeds (Fig. 4c and d). Moreover, consistent with the $OsCAD1^{H25R}$ allele in *spl17*, expression of the mutant $OsCAD1^{D8}$ allele was significantly reduced relative to the wild-type allele in Nipponbare (Figs. 3e and 4e). Disease assessment further demonstrated that, similar to the *spl17* plants, the $OsCAD1^{D8}$ mutant exhibited enhanced resistance to *X. oryzae* pv. *oryzae* strain $PXO99^{A}$, whereas the Nipponbare cultivar remained susceptible to the pathogen (Figs. 1f and 4f).

N-Terminally Tagged OsCAD1 Proteins Exhibit Ubiquitous Localization in *Nicotiana Benthamiana* Cells and are Detected in Both the Soluble and Membrane-Associated Fractions

The subcellular localization of OsCAD1 was examined in *Nicotiana benthamiana* leaf cells using confocal microscopy following transient expression of eGFP-OsCAD1. Both eGFP-OsCAD1 and eGFP control were broadly distributed throughout the cells, including the nucleus, cytosol, and cytoplasmic membrane (Fig. 5a; Fig. S4). However, a subtle difference in cytosolic distribution was observed: while eGFP was evenly dispersed in the cytosol, eGFP-OsCAD1 displayed a starburst-like pattern surrounding the nucleus, suggesting that a subset of OsCAD1 proteins may associate with intracellular membrane systems (Fig. 5a; Fig. S4). Further confocal analysis showed that only the potentially membrane-associated

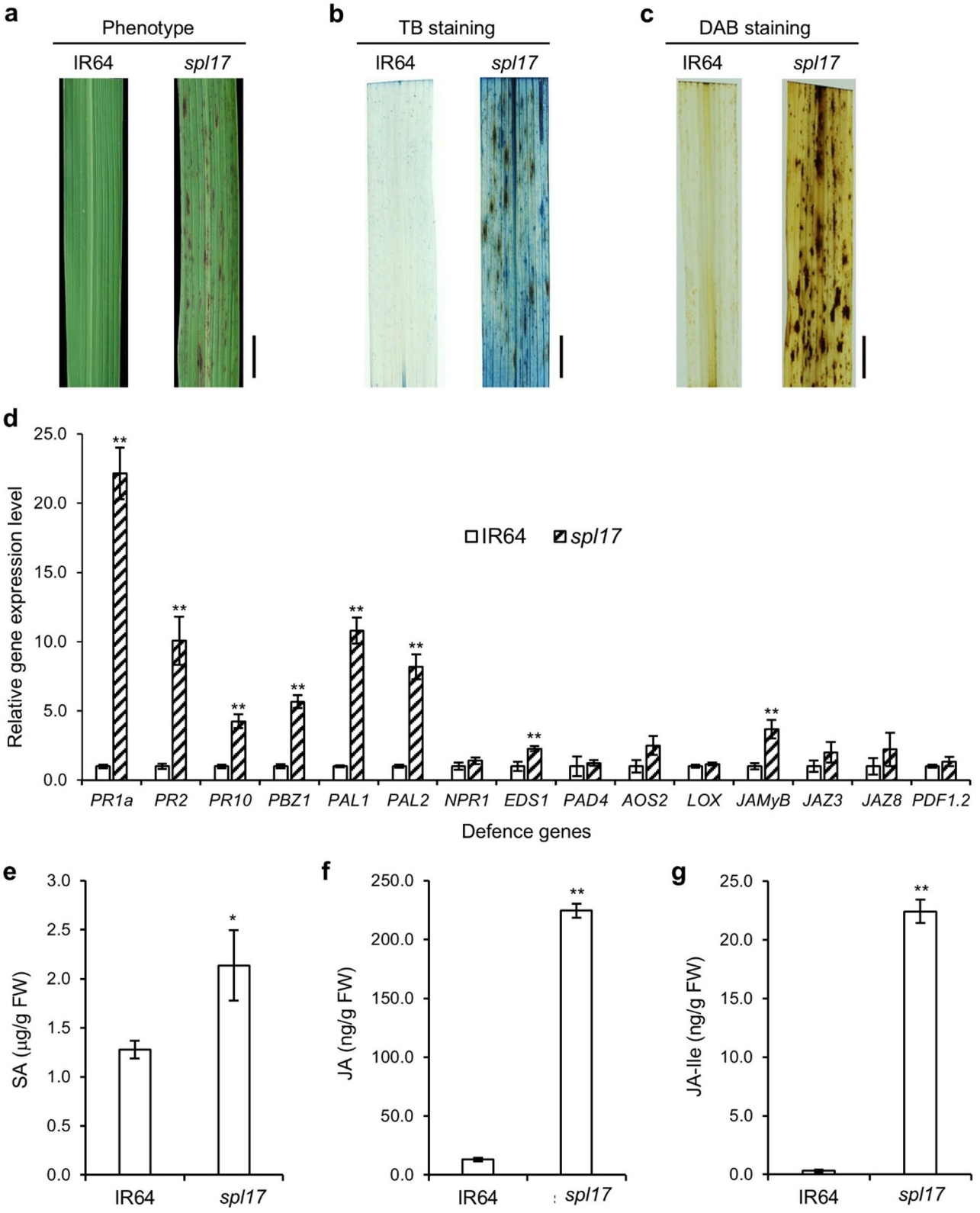

Fig. 2 (See legend on next page.)

(See figure on previous page.)

Fig. 2 Histochemical, molecular, and plant hormone analyses of IR64 and *spl17*.**a** Leaf phenotypes of IR64 and *spl17*. Scale bar = 1 cm. **b** Trypan blue (TB) staining indicating cell death in IR64 and *spl17*. Scale bar = 1 cm. **c** 3,3′-Diaminobenzidine (DAB) staining to detect hydrogen peroxide (H_2O_2) accumulation in IR64 and *spl17*. Scale bar = 1 cm. **d** Relative expression levels of defense-related genes in IR64 and *spl17* as determined by qRT-PCR. Additional information on the defense-related genes is provided in Table S1. **e–g** Quantification of endogenous salicylic acid (SA) (**e**), jasmonic acid (JA) (**f**), and jasmonoyl-isoleucine (JA-Ile) (**g**) levels in IR64 and *spl17*. Hormones were extracted from the leaves of 4-week-old plants and analyzed by liquid chromatography – tandem mass spectrometry (LC-MS/MS) as described in the Materials and Methods. Error bars represent standard deviations (SD). Data represent the mean of three biological replicates per genotype. Asterisks in (**d**) to (**g**) indicate statistically significant differences between IR64 and *spl17* (** $p \leq 0.01$, $0.01 <$ * $p \leq 0.05$; Student's *t*-test)

eGFP-OsCAD1, and not the cytosolic or nuclear-localized forms, co-localized with the endoplasmic reticulum (ER) membrane marker mCherry-RcDGAT2 (Fig. 5b). Western blot analysis confirmed the presence of both eGFP-OsCAD1 and eGFP at their expected molecular weights in total protein extracts from agroinfiltrated *N. benthamiana* leaves (Fig. 5c). A construct expressing OsCAD1 fused to a C-terminal eGFP tag (OsCAD1-eGFP) was generated to assess tag position effects; however, no fluorescence was detected by confocal microscopy (data not shown). To investigate whether the C-terminal tag influenced OsCAD1 expression or stability, a 4×HA tag was fused to either the N- or C-terminus of OsCAD1. Western blotting revealed that only the N-terminally tagged 4×HA-OsCAD1 was detectable in both soluble and membrane-associated fractions (Fig. 5d), indicating OsCAD1's presence in cytosolic/nuclear soluble compartments and membrane-bound fractions, particularly those associated with the ER. Conversely, the C-terminally tagged OsCAD1-4×HA was scarcely detectable in either fraction (Fig. 5d).

Genes Involved in Stress Responses, Signaling Pathways, and Metabolic Processes are Differentially Expressed in IR64 and *spl17*

To investigate the role of *OsCAD1* in stress responses, signaling pathways, and metabolic processes, RNA-Seq analysis was performed to compare the whole-genome transcriptomes of IR64 and *spl17*. A total of 1,466 genes were downregulated and 1,927 genes were upregulated in *spl17* relative to IR64 (Table S4). Differentially expressed genes (DEGs) were grouped based on expression similarity, with downregulated and upregulated genes forming distinct clusters (Fig. S5). High reproducibility was observed across biological replicates. Among the 3,393 DEGs, several gene families exhibited substantial transcriptional alterations attributable to the $OsCAD1^{H25R}$ mutation. The top 15 most affected families/clusters included genes encoding disease resistance proteins, WRKY transcription factors, E3 ubiquitin–protein ligases, UDP-glycosyltransferases, GDSL esterases/lipases, and receptor kinases (Fig. 6a). Most of these gene families showed a predominance of upregulated over downregulated genes, except for GDSL esterase/lipases and photosystem I/II-related genes, which were primarily downregulated. These patterns suggest that stress response and signaling-related genes are transcriptionally activated in *spl17*, whereas genes associated with growth and photosynthesis are repressed. Among the 50 DEGs associated with disease resistance, 39 were upregulated in *spl17* (Fig. 6a). In addition, nine pathogenesis-related (PR) genes, including *PR1a* and *PR10*, were upregulated, and their expression patterns were confirmed by qRT-PCR (Fig. 2d). This transcriptional upregulation likely contributes to the enhanced resistance of *spl17* to *X. oryzae* pv. *oryzae* (Fig. 1f).

Five previously characterized lesion mimic-associated genes, *FGL* (*Os10g0496900*), *OsHPL3* (*Os02g0110200*), *XB15* (*Os03g0821300*), *Spl7* (*Os05g0530400*), and *LIL1/ALS1* (*Os07g0488400*), were also differentially expressed in *spl17* (Fig. 6b). *FGL* and *OsHPL3* were downregulated, whereas *XB15*, *Spl7*, and *LIL1/ALS1* were upregulated. *FGL* encodes protochlorophyllide oxidoreductase B, which is essential for chlorophyll biosynthesis, and mutations in *FGL* result in leaf variegation and lesion formation (Sakuraba et al. 2013). *OsHPL3* encodes a fatty acid 13-hydroperoxide lyase, and loss-of-function mutants display lesion mimic phenotypes (Liu et al. 2012; Tong et al. 2012) *Spl7* encodes a heat stress-responsive transcription factor that, when overexpressed, induces lesion mimic phenotypes associated with hydrogen peroxide accumulation (Yamanouchi et al. 2002; Hoang et al. 2019). *XB15* encodes a PP2C-type phosphatase that functions as a negative regulator of cell death and XA21-mediated immune signaling (Park et al. 2008). *LIL1/ALS1* encodes a cysteine-rich receptor-like kinase, and mutations in this gene result in lesion mimic phenotypes accompanied by upregulation of the mutant alleles (Zhou et al. 2017; Du et al. 2019). The observed downregulation of *FGL* and *OsHPL3* and upregulation of *Spl7* are likely to promote cell death and lesion formation in *spl17*. However, the roles of *XB15* and *LIL1/ALS1* in these processes warrant further investigation.

Comparative Analysis of the Functional Specificities of DEGs Between IR64 and *spl17*

To investigate the functional distinctions between DEGs and the total set of expressed genes, Gene Set Enrichment Analysis (GSEA) was performed as described in the Methods section. Gene Ontology (GO) terms were assigned to both groups to identify over-represented functional categories through proportion-based analysis.

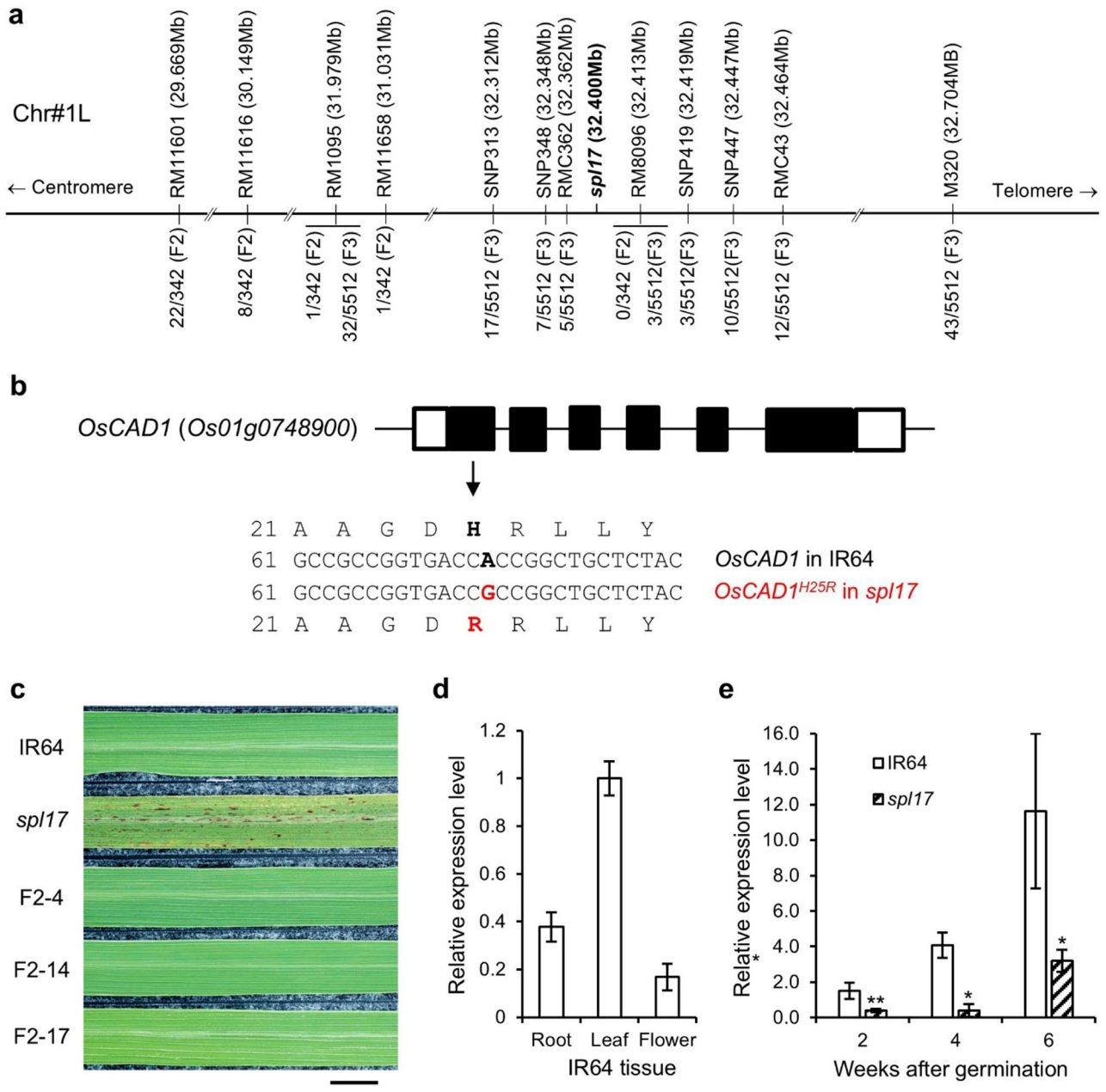

Fig. 3 Map-based cloning of *spl17*. **a** Genetic mapping of the *spl17* locus. The upper panel shows molecular markers and their physical positions on rice chromosome 1, while the lower panel presents the mapping populations and the corresponding recombinants detected by individual molecular markers in each population. The diagram is not drawn to scale. **b** Gene structure of *OsCAD1* (*Os01g07489007*) and sequence alignment of the *OsCAD1* and *OsCAD1*^{H25R} alleles at the mutation site. The schematic illustrates coding regions (filled boxes) and untranslated regions (open boxes) at the 5′ and 3′ ends. The alignment compares the amino acid and codon sequences of the *OsCAD1* allele from IR64 (top) with the *OsCAD1*^{H25R} allele from *spl17* (bottom), highlighting a histidine-to-arginine substitution that gives rise to the *OsCAD1*^{H25R} protein variant. Numbers indicate amino acid residues or nucleotide positions within the open reading frame. **c** Leaf phenotypes of IR64, *spl17*, and three independent complementation lines (F2-4, F2-14, and F2-17) in the *spl17* genetic background. Scale bar = 1 cm. **d** Relative expression levels of *OsCAD1* in different tissues of IR64. **e** Relative expression levels of *OsCAD1* in IR64 and *OsCAD1*^{H25R} in *spl17* at different developmental stages. Gene expression in (**d**) and (**e**) was quantified by qRT-PCR and normalized to the expression of the rice elongation factor gene *OsEF-1α* (*Os03g0178000*). Asterisks in (**e**) indicate statistically significant differences between IR64 and *spl17* (**$p \le 0.01$, $0.01 < *p \le 0.05$; Student's *t*-test)

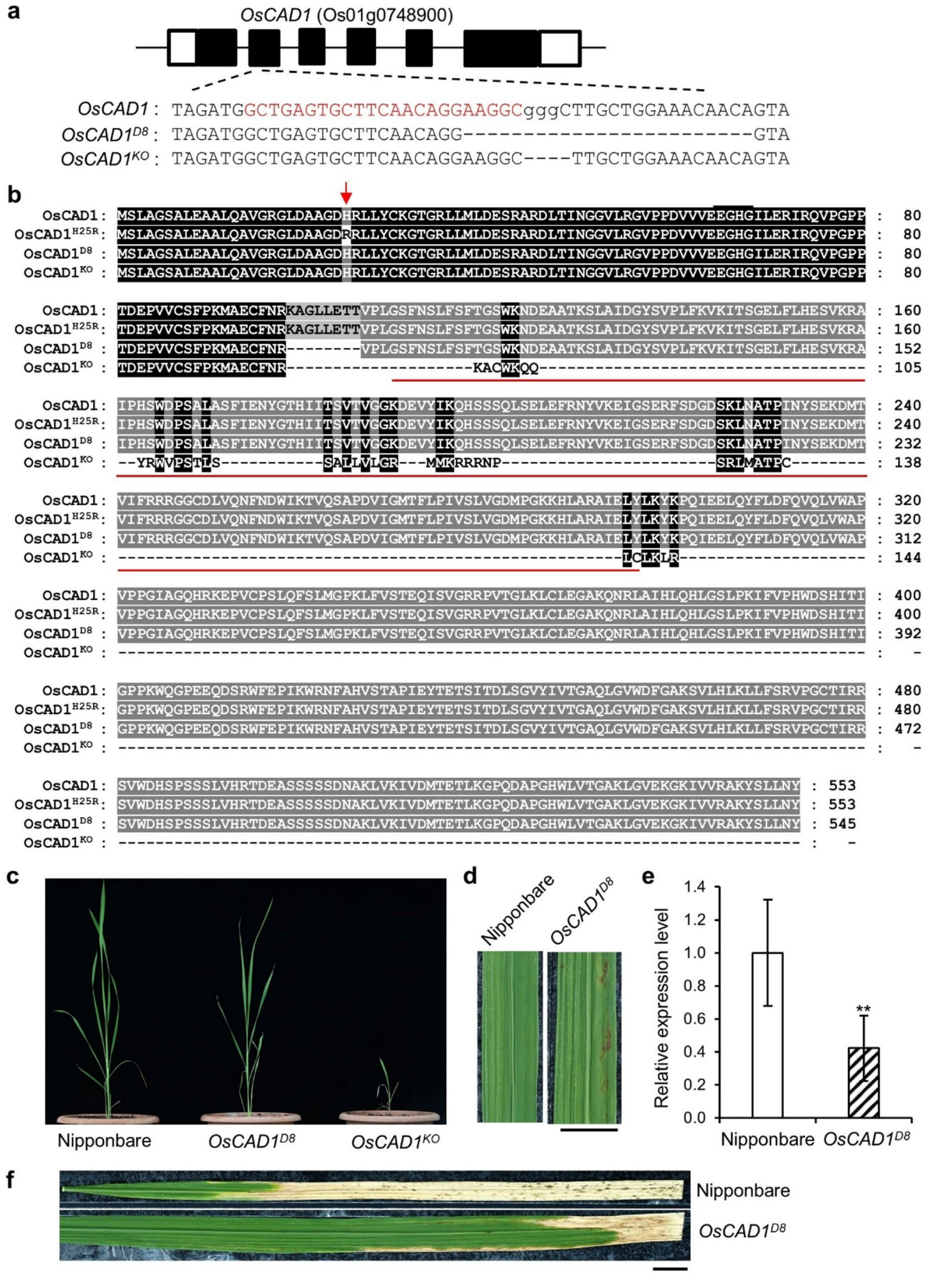

Fig. 4 (See legend on next page.)

(See figure on previous page.)

Fig. 4 Generation of *OsCAD1* mutants via CRISPR/Cas9-mediated genome editing. **a** CRISPR/Cas9-mediated editing of *OsCAD1* in Nipponbare. The schematic diagram depicts the gene structure of *OsCAD1*, with untranslated regions (UTRs), exons, and introns represented by open boxes, black boxes, and lines, respectively. The nucleotide sequences of the CRISPR/Cas9 target site (highlighted in red) and the protospacer adjacent motif (PAM) in Nipponbare, as well as the corresponding sequences of the CRISPR/Cas9-induced *OsCAD1* mutant alleles, are shown below. Deletions are indicated by dashes. $OsCAD1^{D8}$ denotes a mutant allele containing a 24-bp deletion, whereas $OsCAD1^{KO}$ carries a 4-bp deletion. **b** Amino acid sequence alignment of *OsCAD1* and its mutant variants. Sequences were aligned using the MAFFT algorithm implemented in MegAlign Pro and visualized with GeneDoc. Highly conserved residues across all aligned sequences are highlighted in black, whereas residues conserved in the majority of sequences are shaded in grey. $OsCAD1^{KO}$ and $OsCAD1^{D8}$ represent two CRISPR/Cas9-induced mutant variants of *OsCAD1*. The membrane attack complex/perforin (MACPF) domains are indicated by red underlining. The red arrow denotes the amino acid substitution distinguishing *OsCAD1* from the mutant variant $OsCAD1^{H25R}$. **c** Phenotypic comparison between Nipponbare and CRISPR/Cas9-induced *OsCAD1* mutants The photograph was taken 18 days after germination to illustrate morphological differences. **d** Leaf phenotypes of IR64, *spl17*, Nipponbare, and $OsCAD1^{D8}$. The photograph was taken two months after germination. Scale bar = 1 cm. **e** Relative expression levels of *OsCAD1* in Nipponbare and the $OsCAD1^{D8}$ mutant. Gene expression in leaf tissues of 4-week-old plants was quantified by qRT-PCR and normalized to the rice elongation factor gene *OsEF-1α* (*Os03g0178000*). Asterisks indicate statistically significant differences between Nipponbare and $OsCAD1^{D8}$ (**$p \leq 0.01$; Student's *t*-test). **f** Bacterial blight symptoms in Nipponbare and $OsCAD1^{D8}$. Leaves were photographed two weeks after inoculation with *X. oryzae* pv. *oryzae* strain $PXO99^{A}$. At least nineteen leaves from four individual plants were inoculated per experiment. The experiment was repeated three times with similar results. Representative data are shown. Scale bar = 1 cm

GO terms were classified into three categories: Molecular Function (MF), Biological Process (BP), and Cellular Component (CC) (Ashburner et al. 2000), with the aim of determining whether DEGs exhibit functional enrichment.

In the MF category, 1,407 out of the 3,393 DEGs were annotated with GO terms. Statistical analysis identified 37 significantly over-represented GO terms (adjusted $p < 0.05$), with the top 20 presented in Fig. 7a and their corresponding *p*-values shown in Fig. S6. The most enriched term was catalytic activity (GO:0003824), present in 62.5% of DEGs (879/1,407) compared to 51.3% of all expressed genes (9,498/18,515), indicating elevated expression of genes with enzymatic functions in *spl17*. Hierarchical clustering of the top 20 GO terms further grouped them into antioxidant activity, binding, and catalytic activity categories (Fig. S7a). Notably, only one term, peroxidase activity, (GO:0004601), was related to antioxidant functions, whereas the majority were associated with binding (8 terms) and catalytic activity (10 terms). These results suggest that DEGs predominantly encode proteins involved in oxidation-reduction processes, ion binding, and enzymatic functions.

In the BP category, 1,235 DEGs were annotated with GO terms. GSEA identified 62 significantly enriched GO terms (adjusted $p < 0.05$), with the top 20 shown in Fig. 7b and detailed statistics in Fig. S8. Each enriched GO term was more frequently represented among DEGs than in the background gene set, reflecting altered biological functions in the *spl17* mutant. A hierarchical view grouped these terms into metabolic processes, cellular processes, and responses to stimuli, with 8, 9, and 3 GO terms in each category (Fig. S7b), respectively. These findings suggest that DEGs are involved in key biological pathways such as terpenoid biosynthesis, light-harvesting in photosynthesis, detoxification, and stress responses.

In the CC category, 1,245 DEGs were assigned GO terms. GSEA identified 34 significantly over-represented terms (adjusted $p < 0.05$), with the top 20 displayed in Fig. 7c and their *p*-values in Fig. S9. Several membrane-associated GO terms, including cell periphery (GO:0071944), plasma membrane (GO:0005886), intrinsic component of membrane (GO:0031224), and integral component of membrane (GO:0016021), were significantly enriched, indicating substantial involvement of DEGs in membrane-related functions. Tree-based classification further grouped these terms into cell periphery (4 terms), extracellular region (2 terms), and organelles (14 terms) (Fig. S7c), suggesting a significant association of DEGs with membrane processes and organelles, particularly those linked to photosynthesis.

Collectively, these results indicate that DEGs between IR64 and *spl17* are functionally enriched in categories related to catalytic activity, metabolic processes, and membrane-associated functions, reflecting potential shifts in cellular activity and physiological state associated with the *OsCAD1* mutation.

Discussion

In this study, we cloned and characterized the rice lesion mimic gene *spl17*, identifying a weak allele, $OsCAD1^{H25R}$, that promotes ROS accumulation, elevates SA and JA levels, and constitutively activates defense-related genes. These molecular changes ultimately lead to lesion formation as a result of cell death. Functional characterization through gene-editing experiments revealed that $OsCAD1^{H25R}$ is a hypomorphic allele, as complete knockout of *OsCAD1* ($OsCAD1^{KO}$) induced severe cell death and seedling lethality (Fig. 4c). Consistent with our findings, Wang et al. (2025) recently reported another weak allele of *OsCAD1*, designated *oscad1*, which encodes the $OsCAD1^{F416L}$ variant and exhibits lesion mimic phenotypes through an SA-dependent pathway. Gene-edited knockout lines generated in that study likewise exhibited seedling lethality. The variation in lesion severity and cell death phenotypes observed among *OsCAD1* knockdown and knockout mutants, both in Wang et al. (2025) and in our work, is comparable to that reported for *AtCAD1*

mutants in *Arabidopsis* (Morita-Yamamuro et al. 2005; Holmes et al. 2021). The lethality observed in knockouts underscores the essential roles of both *AtCAD1* and *OsCAD1* in maintaining plant viability and modulating defense activation. These findings point to the broader biological significance of membrane-attack complex/perforin (MACPF) domain-containing proteins in plant development and immunity, warranting further research into their molecular and biochemical mechanisms.

Interestingly, both the $OsCAD1^{H25R}$ allele in *spl17* and the $OsCAD1^{D8}$ allele in a separate genome-edited line exhibited significantly lower transcript levels compared to their wild-type counterparts in IR64 and Nipponbare, respectively (Figs. 3e and 4e). Holmes et al. (2021) previously demonstrated that the *cad11-5* allele in *Arabidopsis* compromises the stability and accumulation of the corresponding $AtCAD1^{C43Y}$ protein. Similarly, Wang et al. (2025) reported that although transcript levels of $OsCAD1^{F416L}$ were elevated, protein levels were reduced relative to wild-type, suggesting possible post-transcriptional regulation. Collectively, these findings suggest that mutations in *AtCAD1* or *OsCAD1* may alter transcript abundance or protein stability through currently unidentified mechanisms, potentially involving the degradation of toxic mutant proteins or the repression of mutant gene expression.

Subcellular localization analyses showed that N-terminally tagged OsCAD1 proteins were ubiquitously distributed in *N. benthamiana* cells and were present in both soluble and membrane-associated fractions (Fig. 5a and d). In contrast, no fluorescence was detected from C-terminal OsCAD1-eGFP constructs under confocal microscopy (data not shown), and C-terminally tagged OsCAD1-4×HA was barely detectable by western blotting (Fig. 5d). These findings differ from those of Wang et al. (2025), who reported broad OsCAD1-GFP localization in both rice protoplasts and *N. benthamiana* cells. These findings also contrast with observations in *Arabidopsis*, where AtCAD1-GFP retains functional activity, whereas GFP-AtCAD1 exhibits dominant-negative effects in both the *cad1-5* mutant and the Col-0 background (Holmes et al. 2021). Notably, OsCAD1 features a shorter N-terminal region than AtCAD1 and polymorphisms in amino acid residues 488–508 (Fig. S1). Whether these structural differences affect the stability or function of tagged proteins remains an open question requiring further investigation.

Lesion development in *spl17* is strictly light-dependent (Fig. 1c), and ROS accumulation closely correlates with cell death and lesion formation (Fig. 2b – c). Transcriptomic (RNA-Seq) and gene set enrichment analyses (GSEA) identified DEGs between IR64 and *spl17* that are involved in light harvesting, hydrogen peroxide catabolism, detoxification processes, and responses to environmental stress and toxic compounds (Fig. 7b; Fig. S7b). As ROS are intrinsic byproducts of oxygenic photosynthesis, the balance between light capture and detoxification influences the onset of PCD. While efficient detoxification mechanisms protect against photooxidative damage, their impairment can trigger PCD as a form of stress adaptation. Although the precise relationship between the $OsCAD1^{H25R}$ mutation and ROS accumulation remains unclear, insights may be drawn from *Arabidopsis* studies on singlet oxygen ($^1O_2$), the most reactive form of ROS. Under excessive light, $^1O_2$ causes oxidative damage to proteins, lipids, and DNA, leading to decreased photosynthetic efficiency and cell death (Laloi and Havaux 2015). To mitigate these effects, plants deploy $^1O_2$-scavenging systems involving carotenoids, tocopherols, plastoquinones, and antioxidants like ascorbate, ubiquinol, and glutathione (Krieger-Liszkay et al. 2008; Pinnola and Bassi 2018). Elevated $^1O_2$ levels have been reported in *Arabidopsis* mutants such as *ch1* and *flu* (op den Camp et al. 2003; Ramel et al. 2013). Beyond its cytotoxic effects, $^1O_2$ also functions as a signaling molecule that regulates nuclear gene expression and modulates phytohormone signaling pathways, including those involving ethylene, JA, and SA, ultimately influencing PCD (Danon et al. 2005).

In the *spl17* mutant, $OsCAD1^{H25R}$ leads to elevated levels of SA, JA, and JA-Ile, along with the upregulation of genes associated with SA, JA, and ethylene biosynthesis and signaling (Figs. 2d and g and 6a). In *Arabidopsis*, SA is required for lesion mimic phenotypes in *cad1-1* and *nsl1-1* mutants, and unpublished data suggest JA accumulation and activation of JA/ethylene-responsive genes in *cad1-1* as well (Morita-Yamamuro et al. 2005; Noutoshi et al. 2006). JA plays a central role in plant responses to biotic and abiotic stress via complex hormonal crosstalk (Yang et al. 2019). The increased JA and JA-Ile levels in both *cad1-1* and *spl17* suggest that *AtCAD1* and *OsCAD1* may also mediate abiotic stress tolerance. Supporting this, *AtCAD1* has been shown to enhance osmotic stress tolerance by modulating defense pathways (Murakoshi et al. 2024), and expression of *AtNSL1* and *AtCAD1* is induced by salt stress but not by *Pseudomonas syringae* infection (Noutoshi et al. 2006). These findings indicate that constitutive defense activation may not represent the primary role of MACPF proteins but rather a consequence of disrupted stress regulation. In the *spl17* mutant, impaired detoxification of ROS under light exposure may act as the initial trigger for cell death, while the subsequent activation of defense responses and developmental abnormalities likely represent downstream or concomitant effects. Therefore, further investigation is warranted into the role of MACPF proteins in modulating ROS levels, particularly $^1O_2$, and the associated signaling pathways under light-induced stress conditions.

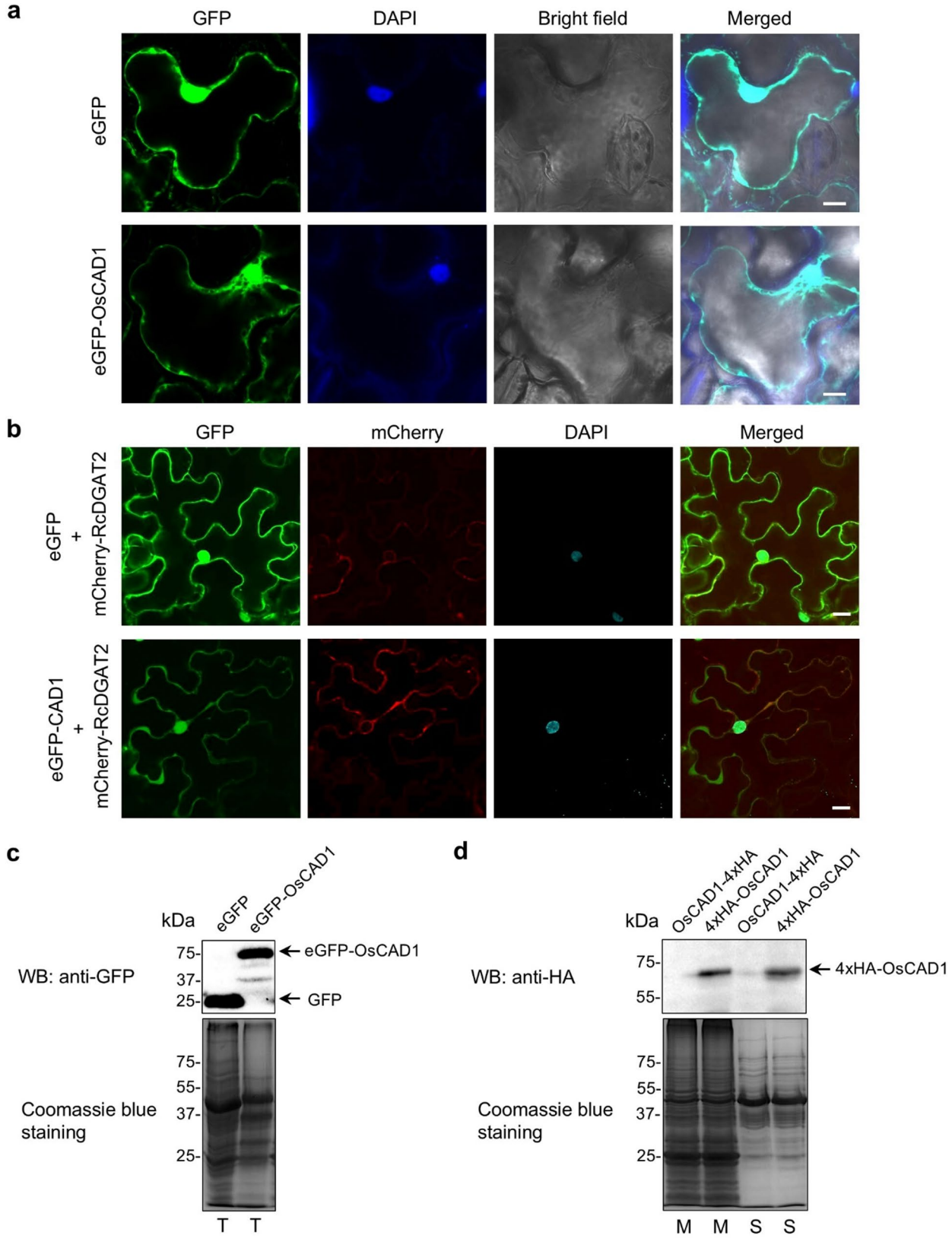

Fig. 5 (See legend on next page.)

(See figure on previous page.)

Fig. 5 Subcellular localization of epitope-tagged *OsCAD1* in *Nicotiana benthamiana* cells. **a** Confocal microscopy images of *N. benthamiana* cells expressing eGFP or eGFP-tagged OsCAD1. Scale bar = 10 μm. **b** Confocal microscopy images of *N. benthamiana* cells co-expressing eGFP or eGFP-OsCAD1 and mCherry-tagged RcDGAT2. Scale bar = 10 μm. **c** Western blot analysis of eGFP and eGFP-OsCAD1 proteins transiently expressed in *N. benthamiana*. Total proteins (T) were extracted from leaf tissues two days after infiltration with *A. tumefaciens* strain GV3101 carrying either the P_{35S}*:eGFP:* T_{Nos} or P_{35S}*:eGFP-OsCAD1:*T_{Nos} construct. **d** Western blot analysis of OsCAD1-4×HA and 4×HA-OsCAD1 proteins transiently expressed in *N. benthamiana*. Soluble (S) and membrane (M) protein fractions were isolated from leaves two days after infiltration with *A. tumefaciens* strain GV3101 harboring either the P_{35S}*:OsCAD1-4×HA:* T_{Nos} or P_{35S}*:4×HA-OsCAD1:*$T_{Nos.}$ construct. Coomassie Brilliant Blue staining of duplicate SDS-PAGE gels was used as a protein loading control in panels (**c**) and (**d**)

Transcriptomic profiling revealed widespread changes in the expression of genes related to stress, signaling, and metabolism, including the top 15 gene families or clusters (Fig. 6a). These include genes encoding R proteins, PR proteins, and others previously linked to lesion mimic phenotypes. In addition, GSEA identified DEGs enriched in terpenoid biosynthesis and metabolism (Fig. 7b; Fig. S7b), which play key roles in catalytic activity, ion binding, antioxidant function, and membrane-associated processes essential for photosynthesis. Terpenoids, the largest class of plant secondary metabolites, function as potent antioxidants that enhance stress resilience (Isah 2019; Li et al. 2023). Therefore, changes in their biosynthesis likely contribute to the altered stress responses and defense mechanisms observed in *spl17*.

In summary, we identified $OsCAD1^{H25R}$, a weak allele of the MACPF-domain gene *OsCAD1*, as the causal mutation in the *spl17* rice lesion mimic mutant. This mutation results in light-dependent lesion formation and cell death, likely due to disrupted ROS homeostasis during photosynthesis. The mutant also exhibits elevated hormone levels and constitutive activation of defense pathways. Together with the recently reported $OsCAD1^{F416L}$ allele (Wang et al. 2025), our findings establish a foundation for further investigations into the roles of MACPF proteins in coordinating plant immunity, development, and stress tolerance.

Materials and methods

Rice Lines and Growth Conditions

The rice lesion mimic mutant *spl17* is a DEB-induced mutant in the IR64 genetic background (D256) (Wu et al. 2008). The indica cultivar 4183, a wide-compatibility restorer line, was used to generate mapping populations, while *Oryza sativa* ssp. *japonica* cv. Nipponbare was employed for transformation studies. All rice plants, including transgenic lines, were cultivated in a greenhouse under a 12–13 h photoperiod with day/night temperatures of 30–35 °C and 24–26 °C, respectively. For shading assays, 5–7 cm strips of aluminum foil were used to cover portions of *spl17* leaves at the onset of lesion development. The plants were maintained under natural light conditions for 7 days, after which the foil was removed, and the leaves were re-exposed to light for an additional 7–14 days.

Quantification of JA, JA-Ile, and SA via LC-MS/MS

Approximately 100 mg of frozen leaf tissue was homogenized in liquid nitrogen using a mortar and pestle. Samples were extracted overnight at 4 °C in 0.1% formic acid in methanol, followed by 5 min of ultrasonication. The aqueous phase was lyophilized, reconstituted in 100 μL methanol, and filtered through a PTFE syringe filter. Phytohormone analysis was performed using an Agilent 6495 Triple Quadrupole mass spectrometer coupled with a 1290 Infinity II LC system and a Luna Omega Polar C18 column (100 × 2.1 mm, 1.6 μm; Phenomenex) at 40 °C. Injections of 1 μL were analyzed at a 0.35 mL/min flow rate. Mobile phases consisted of 0.1% formic acid in water (A) and methanol with 0.1% formic acid (B), with the following gradient: 0.5–13 min, 10–95% B; 13–17.1 min, 95% B; 17.1–17.2 min, 95–10% B; 17.2–20 min, 10% B. Multiple reaction monitoring (MRM) was employed with positive ESI for JA-Ile and negative ESI for JA and SA. The MassHunter software (Agilent) was used for quantification. MRM transitions were: JA (209 > 58.9), JA-Ile (324 > 151), and SA (137 > 93), based on authenticated standards.

Trypan Blue and DAB Staining

Cell death and hydrogen peroxide (H_2O_2) accumulation were assessed by trypan blue and 3,3′-diaminobenzidine (DAB) staining, respectively, as described by Tian et al. (2014).

Bacterial Blight Inoculation

Xanthomonas oryzae pv. *oryzae* (Xoo) strains were cultured on PSA medium (10 g/L peptone, 10 g/L sucrose, 1 g/L glutamic acid, 16 g/L agar, pH 7.0) at 28 °C for 48 h. Bacterial suspensions were adjusted to an OD600 of 0.5 in sterile water. Inoculations were conducted on 6-week-old plants using the leaf-clipping method (Kauffman et al. 1973). Disease symptoms were evaluated following Gu et al. (2004).

Molecular Markers and Genetic Mapping

Simple sequence repeat (SSR), single nucleotide polymorphism (SNP), and sequence-tagged site (STS) markers were employed to map the *spl17* locus. Initial mapping utilized 171 F_2 individuals from a cross between *spl17* and 4183 with 80 SSR markers covering all 12 chromosomes (McCouch et al. 2002; Lu et al. 2005).

a

Top 15 gene families/clusters with at least 15 DEGs

Gene family/cluster	Up-regulated DEG	Down-regulated DEG	Total DEG
1. Disease resistance protein	39	11	50
2. WRKY transcription factor	35	2	37
3. E3 ubiquitin-protein ligase	21	6	27
4. UDP-glycosyltransferase	19	6	25
5. GDSL esterase/lipase	8	15	23
6. G-type lectin S-receptor-like serine/threonine-protein kinase	18	5	23
7. Photosystem I or II related protein	0	21	21
8. LRR receptor-like serine/threonine-protein kinase	16	5	21
9. Wall-associated receptor kinase	20	1	21
10. Cysteine-rich receptor-like protein kinase	18	1	19
11. Ethylene-responsive transcription factor	15	4	19
12. L-type lectin-domain containing receptor kinase	17	1	18
13. NAC domain-containing protein	13	5	18
14. U-box domain-containing protein	16	1	17
15. Auxin-responsive protein	11	4	15

b

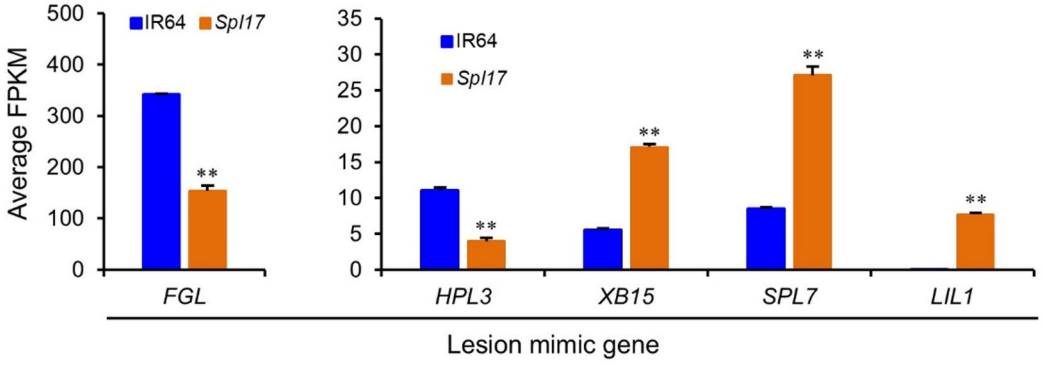

Fig. 6 Comparative expression analysis between IR64 and *spl17* by RNA-Seq. **a** The top 15 gene families with at least 15 DEGs. Abbreviations: UDP, Uridine diphosphate; GDSL, Glycine (G), Aspartic acid (D), Serine (S), and Leucine (L); LRR, Leucine-rich repeat; NAC, no apical meristem (NAM), ATAF1-2 (Arabidopsis Transcription Activator Factor 1–2), and CUC2 (cup-shaped cotyledon). **b** Expression patterns of DEGs associated with mutations that caused lesion mimic phenotypes. Asterisks indicate significant differences between IR64 and *spl17* (**$p < 0.01$ by Student's *t*-test). Abbreviations: FPKM, Fragments Per Kilobase of transcript per Million mapped reads; *FGL*, *Faded Green Leaf*; *HPL3*, *Hydroperoxide Lyase 3*; *XB15*, *XA21 Binding Protein 15*; *SPL7*, *Spotted-leaf 7*; *LIL1*, *Light-Induced Lesion Mimic Mutant 1*

Fine mapping involved 2,756 lesion mimic (homozygous mutant) F_3 plants using two SSRs (RM1095, RM8096), four SNPs (SNP313, SNP348, SNP419, SNP447), and three STS markers (RMC43, RMC362, M320). SSR and STS forward primers were labeled with 6-FAM, and genotyping was conducted on a 3730XL DNA Analyzer. Data were analyzed with GenMapper v3.7 (Applied Biosystems). SNPs were developed from sequence polymorphisms between IR64 and either Shuhui 498 or 4183. Primer sequences for the DNA markers used in this study are provided in Table S1.

Whole-Genome Resequencing

Genomic DNA from IR64 and *spl17* leaves was extracted using the CTAB method. Libraries were prepared and sequenced by BGI Genomics to yield 150-bp paired-end

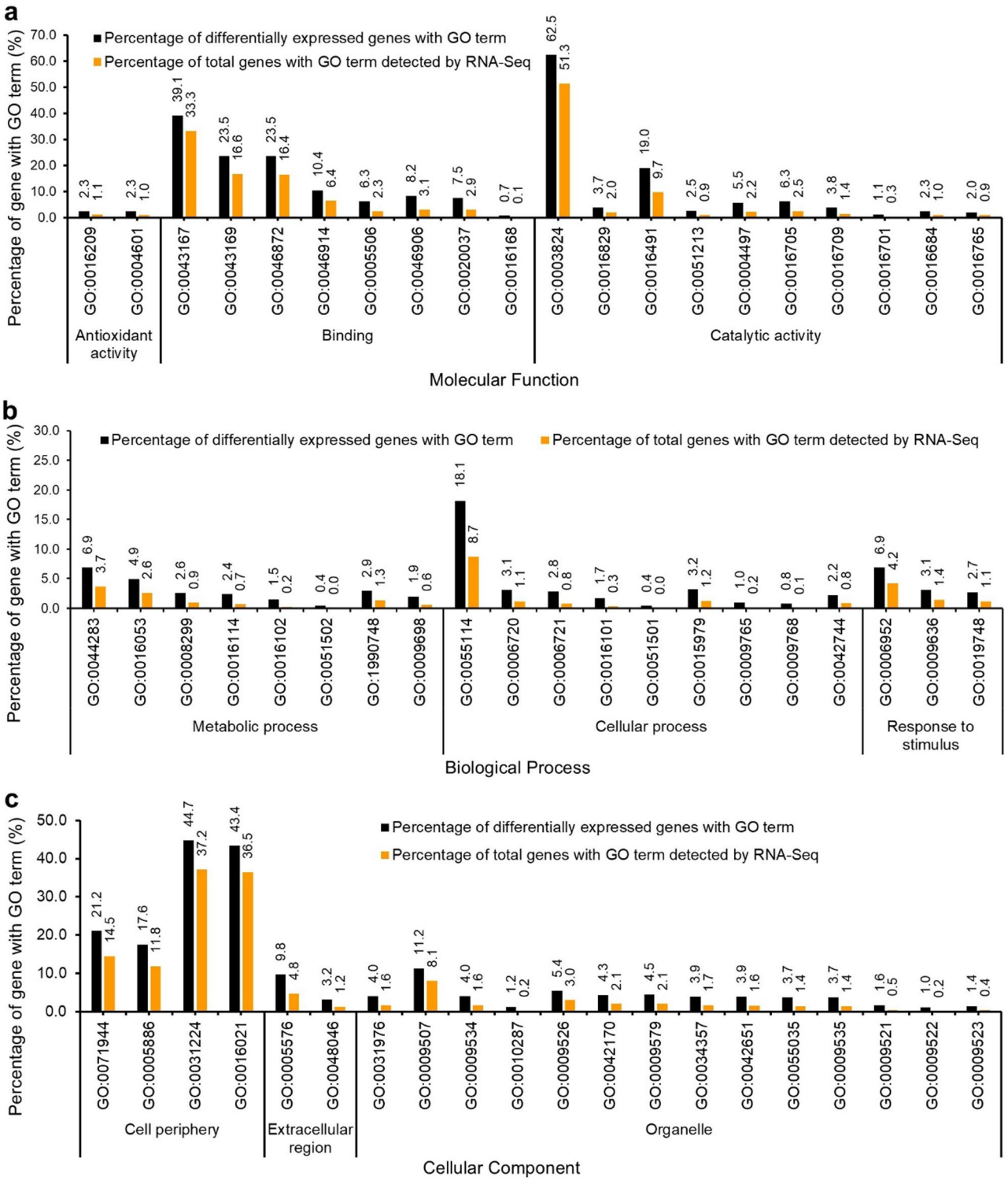

Fig. 7 (See legend on next page.)

reads at ~30× coverage. Reads were aligned to the IR64 reference genome (NCBI: GCA_009914875.1) using BWA-MEM. SAMtools was used for sorting/indexing, and variant calling was performed with GATK.

RACE, RT-PCR, and qRT-PCR

Total RNA was extracted using the FavorPrep™ Plant Total RNA Mini Kit (FAVORGEN). Full-length *OsCAD1* cDNA was obtained through 5′ and 3′ rapid amplification of cDNA ends (RACE) using the SMART RACE

(See figure on previous page.)

Fig. 7 GO term enrichment analysis of DEGs between IR64 and *spl17*.**a** Top 20 enriched molecular function (MF) GO terms among DEGs. Selected enriched GO terms include: GO:0016209 (antioxidant activity), GO:0004601 (peroxidase activity), GO:0043167 (ion binding), GO:0043169 (cation binding), GO:0046872 (metal ion binding), GO:0046914 (transition metal ion binding), GO:0005506 (iron ion binding), GO:0046906 (tetrapyrrole binding), GO:0020037 (heme binding), GO:0016168 (chlorophyll binding), GO:0003824 (catalytic activity), GO:0016829 (lyase activity), GO:0016491 (oxidoreductase activity), GO:0051213 (dioxygenase activity), GO:0004497 (monooxygenase activity), GO:0016705 (oxidoreductase activity, acting on paired donors, with incorporation or reduction of molecular oxygen), GO:0016709 (oxidoreductase activity, acting on paired donors, with incorporation or reduction of molecular oxygen, NAD(P)H as one donor, and incorporation of one atom of oxygen), GO:0016701 (oxidoreductase activity, acting on single donors with incorporation of molecular oxygen), GO:0016684 (oxidoreductase activity, acting on peroxide as acceptor), and GO:0016765 (transferase activity, transferring alkyl or aryl groups other than methyl groups). **b** Top 20 enriched biological process (BP) GO terms among DEGs. Selected GO terms include: GO:0044283 (small molecule biosynthetic process), GO:0016053 (organic acid biosynthetic process), GO:0008299 (isoprenoid biosynthetic process), GO:0016114 (terpenoid biosynthetic process), GO:0016102 (diterpenoid biosynthetic process), GO:0051502 (diterpene phytoalexin biosynthetic process), GO:0019748 (cellular detoxification), GO:0009698 (phenylpropanoid metabolic process), GO:0055114 (oxidation–reduction process), GO:0006720 (isoprenoid metabolic process), GO:0006721 (terpenoid metabolic process), GO:0016101 (diterpenoid metabolic process), GO:0051501 (diterpene phytoalexin metabolic process), GO:0015979 (photosynthesis), GO:0009765 (photosynthesis, light harvesting), GO:0009768 (photosynthesis, light harvesting in photosystem I), GO:0042744 (hydrogen peroxide catabolic process), GO:0006952 (defense response), GO:0009636 (response to toxic substance), and GO:0019748 (secondary metabolic process). **c** Top 20 enriched cellular component (CC) GO terms among DEGs. Selected GO terms include: GO:0071944 (cell periphery), GO:0005886 (plasma membrane), GO:0031224 (intrinsic component of membrane), GO:0016021 (integral component of membrane), GO:0005576 (extracellular region), GO:0048046 (apoplast), GO:0031976 (plastid thylakoid), GO:0009507 (chloroplast), GO:0009534 (chloroplast thylakoid), GO:0010287 (plastoglobuli), GO:0009526 (plastid envelope), GO:0042170 (plastid membrane), GO:0009579 (thylakoid), GO:0034357 (photosynthetic membrane), GO:0042651 (thylakoid membrane), GO:0055035 (plastid thylakoid membrane), GO:0009535 (chloroplast thylakoid membrane), GO:0009521 (photosystem), GO:0009522 (photosystem I), and GO:0009523 (photosystem II)

Kit (Clontech), with primers Spl17-R (5′) and Spl17-F (3′), followed by RT-PCR with primers Spl17-RT-F and Spl17-RT-R. The amplified products were cloned into the pGEM-T Easy vector (Promega) for sequencing. Relative transcript levels were quantified by qRT-PCR using *OsEF-1α* (Os03g0178000) as internal controls. Data were analyzed using the $2^{-\Delta\Delta CT}$ method (Livak and Schmittgen 2001) and are presented as means ± standard deviation from three biological replicates. Primer sequences are listed in Table S3.

Binary Constructs and Rice Transformation

A 6,897-bp genomic fragment of *OsCAD1* (2,640-bp promoter, 2,935-bp coding region, 1,322-bp 3′ region) was cloned from IR64 into pCAMBIA1300 to generate pC1300CAD1 for complementation in Nipponbare. The *eGFP-OsCAD1* fusion gene was inserted into pCAMBIA1305.1 to generate pC35SeGFP-OsCAD1. For subcellular localization, pC35S-mCherry-RcDGAT2 was constructed using a *Ricinus communis* DGAT2 gene (LOC8258757). A sgRNA targeting *OsCAD1* under the rice U6 promoter was cloned into pYLCRISPR/Cas9PUbi-H to create pYLCas9-CAD1 (Ma et al. 2015). Transformation of rice was carried out following the method of Hiei et al. (1994). Primer sequences are listed in Table S3.

Agroinfiltration and Confocal Microscopy in *Nicotiana Benthamiana*

Agrobacterium tumefaciens strain GV3101 carrying binary constructs was infiltrated into *N. benthamiana* leaves as described by Tian et al. (2014). Plants were grown under a 16-h light/8-h dark cycle at 25 °C. Samples were collected 24–48 h post-infiltration for confocal microscopy using a Zeiss LSM 510 Exciter Upright system. Fluorophores were visualized with the following settings: DAPI (405/420–480 nm), GFP (488/500–530 nm), and mCherry (560/570–620 nm). ER labeling was performed via co-expression of mCherry-RcDGAT2.

Protein Extraction and Western Blotting

Total proteins from infiltrated *N. benthamiana* were extracted as described by Gui et al. (2022). Soluble and membrane fractions were isolated using the protocol of Nelson et al. (1984). Tissues were ground in homogenization buffer (18% sucrose, 10 mM $MgCl_2$, 100 mM Tris-HCl pH 8.0, 40 mM β-mercaptoethanol) and centrifuged at 10,000 × *g* for 15 min. The pellet was resuspended in buffer containing 2% SDS, 6% sucrose, and 40 mM β-mercaptoethanol to extract membrane proteins. Western blotting followed Gui et al. (2022).

Transcriptome Analysis and Gene Set Enrichment Analysis (GSEA)

Total RNA from IR64 and *spl17* leaves (three biological replicates each) was extracted using the RNeasy Mini Kit (Qiagen) and sequenced by Macrogen (Seoul, Korea). DEG analysis was performed with DESeq2 (Love et al. 2014), using thresholds of $|\log_2 FC| \geq 1$ and $p < 0.05$. GSEA was conducted based on GO categories for molecular function (MF), biological process (BP), and cellular component (CC) following Subramanian et al. (2005). Enrichment was deemed significant at adjusted $p < 0.05$ and FDR < 0.25. GO annotation and tree visualization were performed using QuickGO (https://www.ebi.ac.uk/QuickGO/) accessed on 25 September 2024.

Supplementary Information

The online version contains supplementary material available at https://doi.org/10.1186/s12284-025-00823-2.

Supplementary material 1.

Supplementary material 2.

Acknowledgements
We respectfully acknowledge the late Dr. Hei Leung for providing the spl17 mutant used in this study. We also thank Dr. Yao-Guang Liu for providing the genome editing vector pYLCRISPR/Cas9PUbi-H, and Dr. Jian-Bo Yang for the rice cultivar 4183.

Author Contributions
DT, YL and ZY designed the research. DT, YL, SJ, YG, RM and IRKP conducted the experiments. DT, YL, IRKP, IJ and ZY analysed the data. DT and ZY wrote the manuscript.

Funding
The work was supported by intramural research funds from Temasek Life Sciences Laboratory.

Data Availability
The raw RNA-Seq data have been deposited in the NCBI database under BioSample accession no. PRJNA1272661.

Declarations

Competing Interests
The authors declare no competing interests.

Received: 17 April 2025 / Accepted: 26 June 2025
Published online: 16 July 2025

References

Alexandersson E, Saalbach G, Larsson C, Kjellbom P (2004) *Arabidopsis* plasma membrane proteomics identifies components of transport, signal transduction and membrane trafficking. Plant Cell Physiol 45:1543–1556
Asada Y, Yamamoto M, Tsutsui T, Yamaguchi J (2011) The *Arabidopsis NSL2* negatively controls systemic acquired resistance via hypersensitive response. Plant Biotechnol 28:9–15
Ashburner M, Ball CA, Blake JA, Botstein D, Butler H, Cherry JM, Davis AP, Dolinski K, Dwight SS, Eppig JT (2000) Gene ontology: tool for the unification of biology. Nat Genet 25:25–29
Balint-Kurti P (2019) The plant hypersensitive response: concepts, control and consequences. Mol Plant Pathol 20:1163–1178
Bigeard J, Colcombet J, Hirt H (2015) Signaling mechanisms in pattern-triggered immunity (PTI). Mol Plant 8:521–539
Bruggeman Q, Raynaud C, Benhamed M, Delarue M (2015) To die or not to die? Lessons from lesion mimic mutants. Front Plant Sci 6:24
Chen T, Nomura K, Wang X, Sohrabi R, Xu J, Yao L, Paasch BC, Ma L, Kremer J, Cheng Y (2020) A plant genetic network for preventing dysbiosis in the phyllosphere. Nature 580:653–657
Cron RQ, Goyal G, Chatham WW (2023) Cytokine storm syndrome. Annu Rev Med 74:321–337
Cui H, Tsuda K, Parker JE (2015) Effector-triggered immunity: from pathogen perception to robust defense. Annu Rev Plant Biol 66:487–511
Danon A, Miersch O, Felix G, op den Camp RG, Apel K (2005) Concurrent activation of cell death-regulating signaling pathways by singlet oxygen in *Arabidopsis thaliana*. Plant J 41:68–80
De Michele R, Vurro E, Rigo C, Costa A, Elviri L, Di Valentin M, Careri M, Zottini M, di Sanita L, Lo Schiavo F (2009) Nitric oxide is involved in cadmium-induced programmed cell death in *Arabidopsis* suspension cultures. Plant Physiol 150:217–228
Du D, Liu M, Xing Y, Chen X, Zhang Y, Zhu M, Lu X, Zhang Q, Ling Y, Sang X (2019) Semi-dominant mutation in the cysteine-rich receptor-like kinase gene, *ALS 1*, conducts constitutive defence response in rice. Plant Biol 21:25–34
Elmore JM, Liu J, Smith B, Phinney B, Coaker G (2012) Quantitative proteomics reveals dynamic changes in the plasma membrane during *Arabidopsis* immune signaling. Mol Cell Proteom 11:M111
Fukunaga S, Sogame M, Hata M, Singkaravanit-Ogawa S, Piślewska-Bednarek M, Onozawa-Komori M, Nishiuchi T, Hiruma K, Saitoh H, Terauchi R (2017) Dysfunction of *Arabidopsis* MACPF domain protein activates programmed cell death via Tryptophan metabolism in MAMP-triggered immunity. Plant J 89:381–393
Gu K, Tian D, Yang F, Wu L, Sreekala C, Wang D, Wang G-L, Yin Z (2004) High-resolution genetic mapping of *Xa27 (t)*, a new bacterial blight resistance gene in rice, *Oryza sativa* L. Theor Appl Genet 108:800–807
Gui Y, Tian D, Ong KH, Teo JCY, Yin Z (2022) TAL effector-dependent *Bax* gene expression in transgenic rice confers disease resistance to *Xanthomonas oryzae* pv. *oryzae*. Transgenic Res: 1–12
Hiei Y, Ohta S, Komari T, Kumashiro T (1994) Efficient transformation of rice (*Oryza sativa* L.) mediated by *Agrobacterium* and sequence analysis of the boundaries of the T-DNA. Plant J 6:271–282
Hoang TV, Vo KTX, Rahman MM, Choi S-H, Jeon J-S (2019) Heat stress transcription factor *OsSPL7* plays a critical role in reactive oxygen species balance and stress responses in rice. Plant Sci 289:110273
Holmes DR, Bredow M, Thor K, Pascetta SA, Sementchoukova I, Siegel KR, Zipfel C, Monaghan J (2021) A novel allele of the *Arabidopsis thaliana* MACPF protein CAD1 results in deregulated immune signaling. Genetics 217:iyab022
Hou X, Wang Y, Qian Q, Ren D (2024) Molecular mechanism of rice necrotic lesion for optimized yield and disease resistance. Rice Sci 31:285–299
Isah T (2019) Stress and defense responses in plant secondary metabolites production. Biol Res 52:39
Kauffman H, Reddy A, Hsieh S, Merca S (1973) An improved technique for evaluating resistance of rice varieties to *Xanthomonas oryzae*. Plant Dis Rep 57:537–541
Krieger-Liszkay A, Fufezan C, Trebst A (2008) Singlet oxygen production in photosystem II and related protection mechanism. Photosynth Res 98:551–564
Laloi C, Havaux M (2015) Key players of singlet oxygen-induced cell death in plants. Front Plant Sci 6:39
Lapin D, Kovacova V, Sun X, Dongus JA, Bhandari D, von Born P, Bautor J, Guarneri N, Rzemieniewski J, Stuttmann J (2019) A coevolved EDS1-SAG101-NRG1 module mediates cell death signaling by TIR-domain immune receptors. Plant Cell 31:2430–2455
Li C, Zha W, Li W, Wang J, You A (2023) Advances in the biosynthesis of terpenoids and their ecological functions in plant resistance. Int J Mol Sci 24:11561
Liu X, Li F, Tang J, Wang W, Zhang F, Wang G, Chu J, Yan C, Wang T, Chu C (2012) Activation of the jasmonic acid pathway by depletion of the hydroperoxide lyase *OsHPL3* reveals crosstalk between the HPL and AOS branches of the Oxylipin pathway in rice. PLoS ONE 7:e50089
Livak KJ, Schmittgen TD (2001) Analysis of relative gene expression data using real-time quantitative PCR and the $2^{-\Delta\Delta CT}$ method. Methods 25:402–408
Lorrain S, Vailleau F, Balagué C, Roby D (2003) Lesion mimic mutants: keys for Deciphering cell death and defense pathways in plants? Trends Plant Sci 8:263–271
Love MI, Huber W, Anders S (2014) Moderated Estimation of fold change and dispersion for RNA-seq data with DESeq2. Genome Biol 15:1–21
Lu H, Redus MA, Coburn JR, Rutger JN, McCouch SR, Tai TH (2005) Population structure and breeding patterns of 145 US rice cultivars based on SSR marker analysis. Crop Sci 45:66–76
Lukoyanova N, Hoogenboom BW, Saibil HR (2016) The membrane attack complex, Perforin and cholesterol-dependent Cytolysin superfamily of pore-forming proteins. J Cell Sci 129:2125–2133
Ma X, Zhang Q, Zhu Q, Liu W, Chen Y, Qiu R, Wang B, Yang Z, Li H, Lin Y (2015) A robust CRISPR/Cas9 system for convenient, high-efficiency multiplex genome editing in monocot and Dicot plants. Mol Plant 8:1274–1284
McCouch SR, Teytelman L, Xu Y, Lobos KB, Clare K, Walton M, Fu B, Maghirang R, Li Z, Xing Y (2002) Development and mapping of 2240 new SSR markers for rice (*Oryza sativa* L). DNA Res 9:199–207
Morita-Yamamuro C, Tsutsui T, Sato M, Yoshioka H, Tamaoki M, Ogawa D, Matsuura H, Yoshihara T, Ikeda A, Uyeda I (2005) The *Arabidopsis* gene *CAD1* controls programmed cell death in the plant immune system and encodes a protein containing a MACPF domain. Plant Cell Physiol 46:902–912
Murakoshi Y, Saso Y, Matsumoto M, Yamanaka K, Yotsui I, Sakata Y, Taji T (2024) *CAD1* contributes to osmotic tolerance in *Arabidopsis thaliana* by suppressing

immune responses under osmotic stress. Biochem Biophys Res Commun 717:150049
Nelson T, Harpster MH, Mayfield SP, Taylor WC (1984) Light-regulated gene expression during maize leaf development. J Cell Biol 98:558–564
Noutoshi Y, Kuromori T, Wada T, Hirayama T, Kamiya A, Imura Y, Yasuda M, Nakashita H, Shirasu K, Shinozaki K (2006) Loss of *necrotic spotted lesions 1* associates with cell death and defense responses in *Arabidopsis thaliana*. Plant Mol Biol 62:29–42
op den Camp RG, Przybyla D, Ochsenbein C, Laloi C, Kim C, Danon A, Wagner D, Hideg É, Göbel C, Feussner I (2003) Rapid induction of distinct stress responses after the release of singlet oxygen in *Arabidopsis*. Plant Cell 15:2320–2332
Park C-J, Peng Y, Chen X, Dardick C, Ruan D, Bart R, Canlas PE, Ronald PC (2008) Rice *XB15*, a protein phosphatase 2 C, negatively regulates cell death and XA21-mediated innate immunity. PLoS Biol 6:e231
Pinnola A, Bassi R (2018) Molecular mechanisms involved in plant photoprotection. Biochem Soc Trans 46:467–482
Ramel F, Ksas B, Akkari E, Mialoundama AS, Monnet F, Krieger-Liszkay A, Ravanat J-L, Mueller MJ, Bouvier F, Havaux M (2013) Light-induced acclimation of the *Arabidopsis* chlorina1 mutant to singlet oxygen. Plant Cell 25:1445–1462
Ruan B, Wu H, Jiang Y, Qiu J, Chen F, Zhang Y, Qiao Y, Tang M, Ma Y, Qian Q (2024) *SPL50* regulates cell death and resistance to *Magnaporthe oryzae* in rice. Rice 17:51
Sakuraba Y, Rahman ML, Cho SH, Kim YS, Koh HJ, Yoo SC, Paek NC (2013) The rice *faded green leaf* locus encodes protochlorophyllide oxidoreductase B and is essential for chlorophyll synthesis under high light conditions. Plant J 74:122–133
Stepp SE, Dufourcq-Lagelouse R, Deist FL, Bhawan S, Certain Sp, Mathew PA, Henter J-I, Bennett M, Fischer A, Basile GS (1999) Perforin gene defects in Familial hemophagocytic lymphohistiocytosis. Science 286:1957–1959
Subramanian A, Tamayo P, Mootha VK, Mukherjee S, Ebert BL, Gillette MA, Paulovich A, Pomeroy SL, Golub TR, Lander ES (2005) Gene set enrichment analysis: a knowledge-based approach for interpreting genome-wide expression profiles. Proc Natl Acad Sci 102:15545–15550
Tian D, Wang J, Zeng X, Gu K, Qiu C, Yang X, Zhou Z, Goh M, Luo Y, Murata-Hori M (2014) The rice TAL effector–dependent resistance protein XA10 triggers cell death and calcium depletion in the Endoplasmic reticulum. Plant Cell 26:497–515
Tong X, Qi J, Zhu X, Mao B, Zeng L, Wang B, Li Q, Zhou G, Xu X, Lou Y (2012) The rice hydroperoxide lyase *OsHPL3* functions in defense responses by modulating the Oxylipin pathway. Plant J 71:763–775
Tsutsui T, Asada Y, Tamaoki M, Ikeda A, Yamaguchi J (2008) *Arabidopsis CAD1* negatively controls plant immunity mediated by both Salicylic acid-dependent and-independent signaling pathways. Plant Sci 175:604–611
Tsutsui T, Morita-Yamamuro C, Asada Y, Minami E, Shibuya N, Ikeda A, Yamaguchi J (2006) Salicylic acid and a Chitin elicitor both control expression of the *CAD1* gene involved in the plant immunity of *Arabidopsis*. Biosci Biotechnol Biochem 70:2042–2048
Wang H, Huang T, Ruan Z, Tu R, He Y, Liu Q, Cheng S, He G, Shen X (2025) A MACPF protein OsCAD1 balances plant growth and immunity through regulating Salicylic acid homeostasis in rice. Plant Cell Environ. https://doi.org/10.1111/pce.15366. published online on 06 January 2025
Wu C, Bordeos A, Madamba MRS, Baraoidan M, Ramos M, Wang G-l, Leach JE, Leung H (2008) Rice lesion mimic mutants with enhanced resistance to diseases. Mol Genet Genomics 279:605–619
Yamanouchi U, Yano M, Lin H, Ashikari M, Yamada K (2002) A rice spotted leaf gene, *Spl7*, encodes a heat stress transcription factor protein. Proc Natl Acad Sci 99:7530–7535
Yang J, Duan G, Li C, Liu L, Han G, Zhang Y, Wang C (2019) The crosstalks between jasmonic acid and other plant hormone signaling highlight the involvement of jasmonic acid as a core component in plant response to biotic and abiotic stresses. Front Plant Sci 10:1349
Yin Z, Chen J, Zeng L, Goh M, Leung H, Khush GS, Wang G-L (2000) Characterizing rice lesion mimic mutants and identifying a mutant with broad-spectrum resistance to rice blast and bacterial blight. Mol Plant Microbe Interact 13:869–876
Yu L, Liu D, Chen S, Dai Y, Guo W, Zhang X, Wang L, Ma S, Xiao M, Qi H (2020) Evolution and expression of the membrane attack complex and Perforin gene family in the Poaceae. Int J Mol Sci 21:5736
Zhang A, Jiang H, Chu H, Cao L, Chen J (2022a) Rice lesion mimic gene cloning and association analysis for disease resistance. Curr Issues Mol Biol 44:2350–2361
Zhang X, Dai Y-S, Wang Y-X, Su Z-Z, Yu L-J, Zhang Z-F, Xiao S, Chen Q-F (2022b) Overexpression of the Arabidopsis MACPF protein AtMACP2 promotes pathogen resistance by activating SA signaling. Int J Mol Sci 23:8784
Zhou Q, Zhang Z, Liu T, Gao B, Xiong X (2017) Identification and map-based cloning of the light-induced lesion mimic mutant 1 (LIL1) gene in rice. Front Plant Sci 8:2122

Publisher's Note

The Histidine-25-Arginine mutation in the rice MACPF protein OsCAD1 induces cell death and activates defense responses in the lesion mimic mutant *spl17*

Supplementary Tables

Table S1. Information on pathogenesis-related and defense-associated genes mentioned in this study

Name	Gene ID	Remark
PR1a	Os07g0129200	Pathogenesis-related gene
PR2	Os01g0944500	Pathogenesis-related gene
PR10	Os12g0555300	Pathogenesis-related gene
PBZ1	Os12g0555500	Pathogenesis-related gene
PAL1	Os02g0626100	SA biosynthesis gene
PAL2	Os02g0626400	SA biosynthesis gene
EDS1	Os09g0392100	SA signaling gene
NPR1	Os01g0194300	SA signaling gene
PAD4	Os11g0195500	SA signaling gene
AOS2	Os03g0225900	JA biosynthesis gene
LOX2	Os08g0508800	JA biosynthesis gene
JAZ3	Os03g0180800	JA signaling gene
JAZ8	Os09g0439200	JA signaling gene
PDF1.2	Os02g0212100	JA signaling gene
JAMyb	Os11g0684000	JA signaling gene

Table S2. Molecular markers on chromosome 1L and their DNA primers

Name	DNA primer (5' to 3')*	Marker type
RM11601	F: GGTGGGAAGCCAACCAGACTCG	SSR marker
	R: GGGTTTACCTGCGCTAACCCAAGC	
RM11616	F: CCGGCTGCACTACCTGTTCACG	SSR marker
	R: GGCGCGAAGTCGTTCCAGTACC	
RM1095	F: CCCATTCAGTTGATCCTGTCTGC	SSR marker
	R: AGCTGGGATGCAGAAGAGTATGG	
RM11658	F: TACCTCGGTGAGATAGGGAATGC	SSR marker
	R: CTTCACATCCACACTTGCACTCG	
RM8096	F: TTATGGACTTGTGGGTGTCATGG	SSR marker
	R: AAAGGCGATGAGTCAACATCTGC	
SNP313	F: AGTGCAACAAAAATTGGCAG	SNP marker
	R: TGACGGCGACACTCAGGGGC	
SNP348	F: TTGAGGTTCTTGAGGCTGCT	SNP marker
	R: CGGGCGAGGAGGGGAGGGAG	
SNP419	F: AGATTCATTCGAGAGCGCGT	SNP marker
	R: TACGTCTTGCTCAGGAACGG	
SNP447	F: GCTACAATGGTACATTTCAC	SNP marker
	R: TGAGTGCTTTGTGCTTGTGG	
RMC43	F: ATGATGGAGGGGATGGAAAT	STS marker
	R: GTCTTCCTACGCTCGGTCAG	
RMC362	F: AACCTCGTCGTCGTGCAAGA	STS marker
	R: TCTCGATCATCCCCTCATCG	
M320	F: CGGCCAAAGTGTATTCCGAC	STS marker
	R: CGGCTCCAAATATCGCCAGT	

*Note: F, forward primer; R, Reverse primer

Table S3. DNA primers and their nucleotide sequences used in this study

Name	Nucleotide sequence (5’ to 3’)	Remark
CAD1Seq-F	GAAGGTGAGGGGAGTTCCC	DNA sequencing and genotyping
CAD1Seq-R	CGCTTAACGCTCTCATGCAGAA	DNA sequencing and genotyping
Spl17-F	AGCGCGCAATTCCACATAGTTG	3’RACE
Spl17-R	CAGGATGCTTCATAGCAGAGTG	5’RACE
Spl17-RT-F	CTCCCCTTCCCGATCAACAG	RT-PCR
Spl17-RT-R	AGGCGCTAATCCCTCACAGAATC	RT-PCR
CAD1-Q-F	CATTGGCTGGTAACAGGAGC	qRT-PCR
CAD1-Q-R	GGATGCTTCATAGCAGAGTG	qRT-PCR
EF-Q-F	GCACGCTCTTCTTGCTTTC	qRT-PCR
EF-Q-R	AGGGAATCTTGTCAGGGTTG	qRT-PCR
CAD1-EcoRI-F	CTCGAGGAATTCTAGAGCACTA	Genetic complementation
CAD1-SalI-R	CTTCAGAATGGTCGACAGAGTTG	Genetic complementation
CAD1-KpnI-R	GACATGGGTACCATAGTTCTCGA	Genetic complementation
CAD1-KpnI-F	GTCGAGAACTATGGTACCCAT	Genetic complementation
GFPCAD1-F	ATGAGCCTCGCTGGCTCCGC	eGFP-OsCAD1 fusion gene
GFPCAD1-R	CAACATGAGCTCAATAGTTTAATAACG	eGFP-OsCAD1 fusion gene
CAD1U6-F	GCCGAGTGCTTCAACAGGAAGGC	Genome editing
CAD1U6-R	AAACGCCTTCCTGTTGAAGCACT	Genome editing
PR1a-F	GGAAGTACGGCGAGAACATC	qRT-PCR
PR1a-R	TGGTCGTACCACTGCTTCTC	qRT-PCR
PR2-F	ATCAACTACGCGCTCTTCACGT	qRT-PCR
PR2-R	GGAGTAGAACGTGTCGACGAT	qRT-PCR
PR4-F	GTGTGGCAAGTGTATCCAGGT	qRT-PCR
PR4-R	CGCAATTATTGTCGCACCTGT	qRT-PCR
PR10-F	CACCATCTACACCATGAAGC	qRT-PCR
PR10-R	CGTCGAGTGCGACTTGAGCTT	qRT-PCR
PBZ1-F	CCCTGCCGAATACGCCTAA	qRT-PCR
PBZ1-R	CTCAAACGCCACGAGAATTTG	qRT-PCR

WRKY45-F	ATTCCACGCGTGTGTACAGA	qRT-PCR
WRKY45-R	TGCTAGCATGTCTGCAGCTT	qRT-PCR
WRKY62-F	GTACCAATGGAGGAAGTACG	qRT-PCR
WRKY62-R	CCACTAGCATTGACCTATCC	qRT-PCR
EDS1-F	CATTCCAAGAACGAGGACACTG	qRT-PCR
EDS1-R	CAAGACTCAAGGCTAGAACCGA	qRT-PCR
NPR1-F	GGATATTGCTCAAGTGGATGG	qRT-PCR
NPR1-R	GTCATCCGAGCTAAGTGTTC	qRT-PCR
PAD4-F	CCAACATGTACCGCATCAAG	qRT-PCR
PAD4-R	TGTAGGTTGTTTCGGTGGTAGT	qRT-PCR
PAL1-F	CTCGGCTGCGTATTCCTCA	qRT-PCR
PAL1-R	GGGATCTTGGCTTAGTTGATG	qRT-PCR
PAL2-F	TCCTGGAGACCTCCATCTTC	qRT-PCR
PAL2-R	CGGCACTCCTTGATCCGGTT	qRT-PCR
PAL5-F	CATCTGCTGATCGAACCAGT	qRT-PCR
PAL5-R	CGTAATCTGCTGATGAGCGT	qRT-PCR
ICS-F	GAGCTTGACCTCAAAGCATC	qRT-PCR
ICS-R	GGAGGTGTTTGATTGATCGG	qRT-PCR
LOX-F	GATGGCGGTGCTCGACGTGCT	qRT-PCR
LOX-R	GCACCTGTTCTTGAGCTTTCTAT	qRT-PCR
AOS2-F	CTCGTCGGAAGGCTGTTGCT	qRT-PCR
AOS2-R	ACGATTGACGGCGGAGGTT	qRT-PCR
JAMyb-F	CCGAGCATGGTGACTAGCTCATCTT	qRT-PCR
JAMyb-R	CCTTGCACCCAACCGTTAAGCTGTT	qRT-PCR
JAZ3-F	TTGGACACATGCACTCGCGC	qRT-PCR
JAZ3-R	GAACCATCTTCCAACTCGAC	qRT-PCR
JAZ8-F	CAGGATGAATGCAAATGCTCC	qRT-PCR
JAZ8-R	AGTGAACTGTAAGCTAAGAGG	qRT-PCR
PDF-F	GACAACGAGTGCATGCTGGA	qRT-PCR
PDF-R	GTCAGGCCAACGTTGCTCAT	qRT-PCR

Supplementary figures

```
OsCAD1 : --------MSLAGS-----ALEAALQAVGRGLDAAGDHRLLYCKGTG--RLLMLDESRARDLTINGGVLR-GVPPDVVVE :  64
AtCAD1 : MENRKGGNFSVPSSEALTTTLRNAIQALGRGFDVTSDVRLLYCKGAPGSRLVRIEEGQNRDLELSHGFLLPNVPADIDCS :  80

OsCAD1 : EGHGILERIRQVPGPPTDEPVVCSFPKMAECFNRKAGLLETTVPLGSFNSLFSFTGSWKNDEAATKSLAIDGYSVPLFKV : 144
AtCAD1 : RGNSGTQRIS-----------VCSFHEMAEEFNVRSG-VKGNIPLGCFNAMFNYTGSWQVDAASTKSLALVGYFIPLYDV : 148

OsCAD1 : KITSGEIPLHESVKRAIPHSWDPSALASFIENYGTHIITSVTVGGKDEVYIKQHSSSQLSELEFRNYVKEIGSERFSDGD : 224
AtCAD1 : KLAKLTIVLHNEIRRAVPSSWDPASLASFIENYGTHIVTSVTIGGRDVVYIRQHQSSPLPVSEIENYVNDMIKHRFHEAE : 228

OsCAD1 : SKLNATPINYSEKDMTVIFRRRGGCDIVQNFNDWIKTVQSAPDVIGMTFLPIVSLVGDMPGKKHIARAIELYLKYKEQIE : 304
AtCAD1 : SQSITGPIKYKDKDITVIFRRRGGDDIEQSHARWAETVPAAPDIINMTFTPIVSLLEGVPGLRHLTRAIELYLEYKEPIE : 308

OsCAD1 : ELQYFLDFQVQLVWAPVPPGIAGQHRKEPVCPSLQFSLMGPKLFVSTEQISVGRRPVTGLKLCLEGAKQNRLAIHLQHLG : 384
AtCAD1 : DLQYFLDYQIARAWAPEQSNLQ---RKEPVCSSLQFSLMGPKLFISADQVTVGRKPVTGLRLSLEGSKQNRLSIHLQHLV : 385

OsCAD1 : SLPKIFVPHWDSHITICPPKWQGPEEQDSRWFEPIKWRNFAHVSTAPIEYTETSITDLSGVYIVTGAQLGVWDFGAKSVL : 464
AtCAD1 : SLPKILQPHWDSHVPICAPKWQGPEEQDSRWFEPIKWKNFSHVSTSPIEHTETHIGDLSGVHIVTGAQLGVWDFGSKNVL : 465

OsCAD1 : HLKLLFSRVPGCTIRRSVWDHSPSSS---LVHRTDEASSS----SSDNAKLVKIVDMTETLKGPQDAPGHWLVTGAKLGV : 537
AtCAD1 : HLKLLFSKVPGCTIRRSVWDHTPVASSGRLEPGGPSTSSSTEEVSGQSGKLAKIVDSSEMLKGPQDLPGHWLVTGAKLGV : 545

OsCAD1 : EKGKIVVRAKYSLLNY : 553
AtCAD1 : EKGKIVLRVKYSLLNY : 561
```

Fig. S1. Amino acid sequence alignment between *AtCAD1* and *OsCAD1*

Amino acid sequences were aligned using MegAlign and visualized with GeneDoc. Identical and conserved residues are highlighted in black. The MACPF domains are underlined in red.

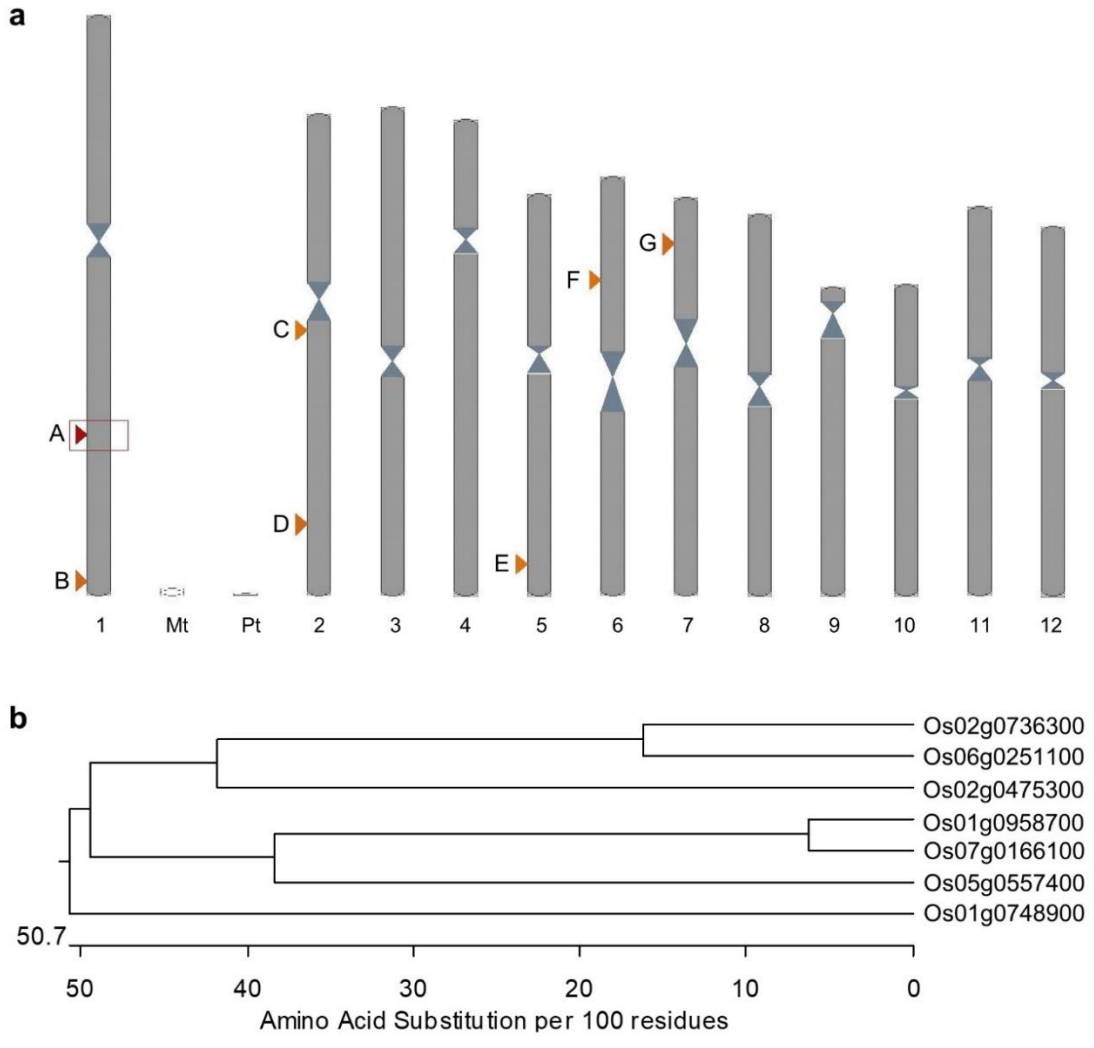

Fig. S2. MACPF family genes in rice

(**a**) Location of MACPF family genes on rice chromosomes. A: *Os01g0748900* (*OsCAD1*); B: *Os01g0958700*; C: *Os02g0475300*; D: *Os02g0736300*; E: *Os05g0557400*; F: *Os06g0251100*; G: *Os07g0166100*.

(**b**) Phylogenetic tree of MACPF family proteins. The phylogenetic tree was generated based on the full-length amino acid sequences using MegAlign Pro with the BIONJ algorithm, uncorrected pairwise distance, and global gap removal. The bar indicates the distance scale.

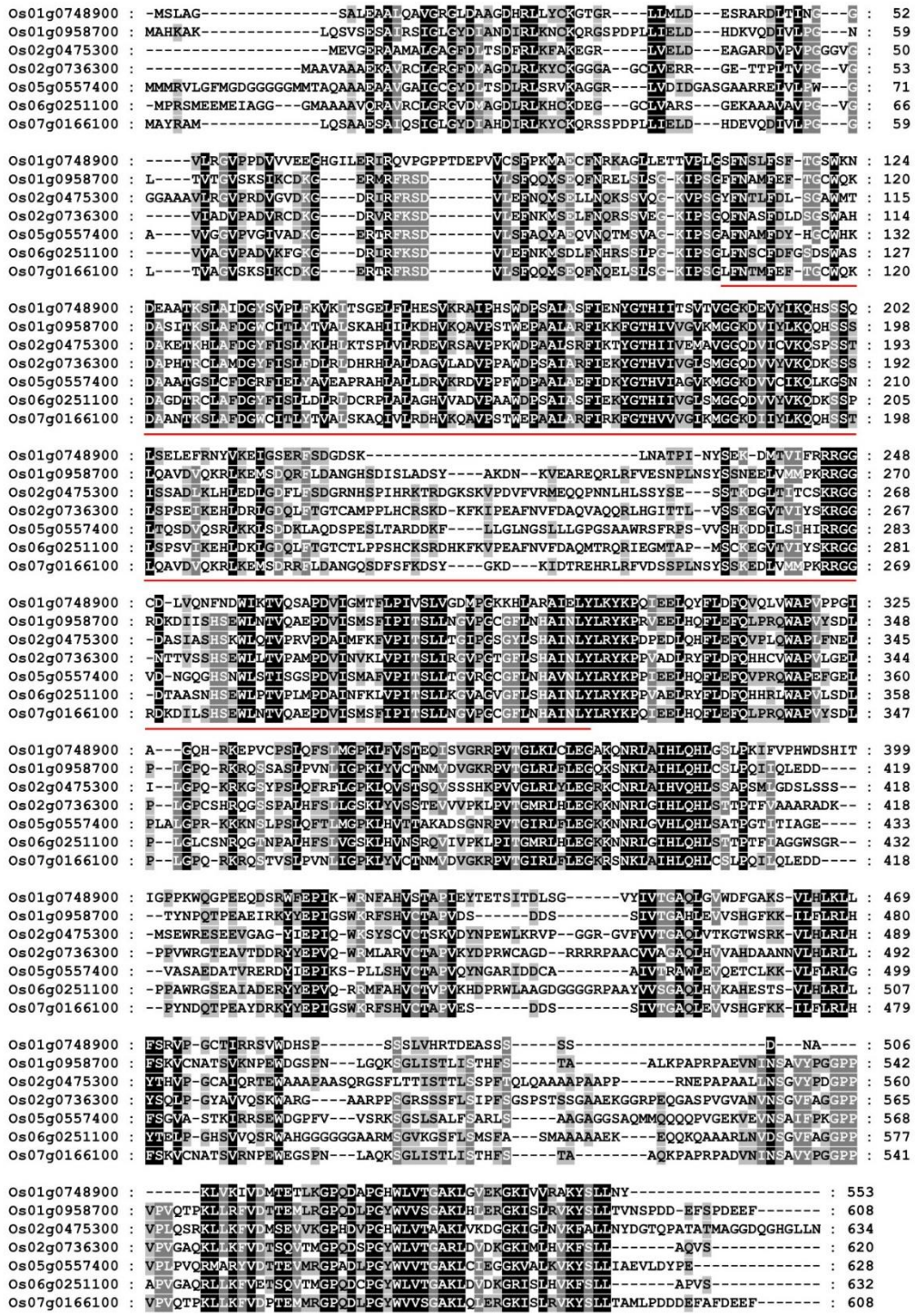

Fig. S3. Amino acid sequence alignment of MAPCF proteins in rice.

The amino acid sequences were aligned using MegAlign software and visualized with GeneDoc. Conserved residues present in all aligned proteins are highlighted in black, while those conserved in most proteins are highlighted in grey. The MACPF domains are indicated with red underlines.

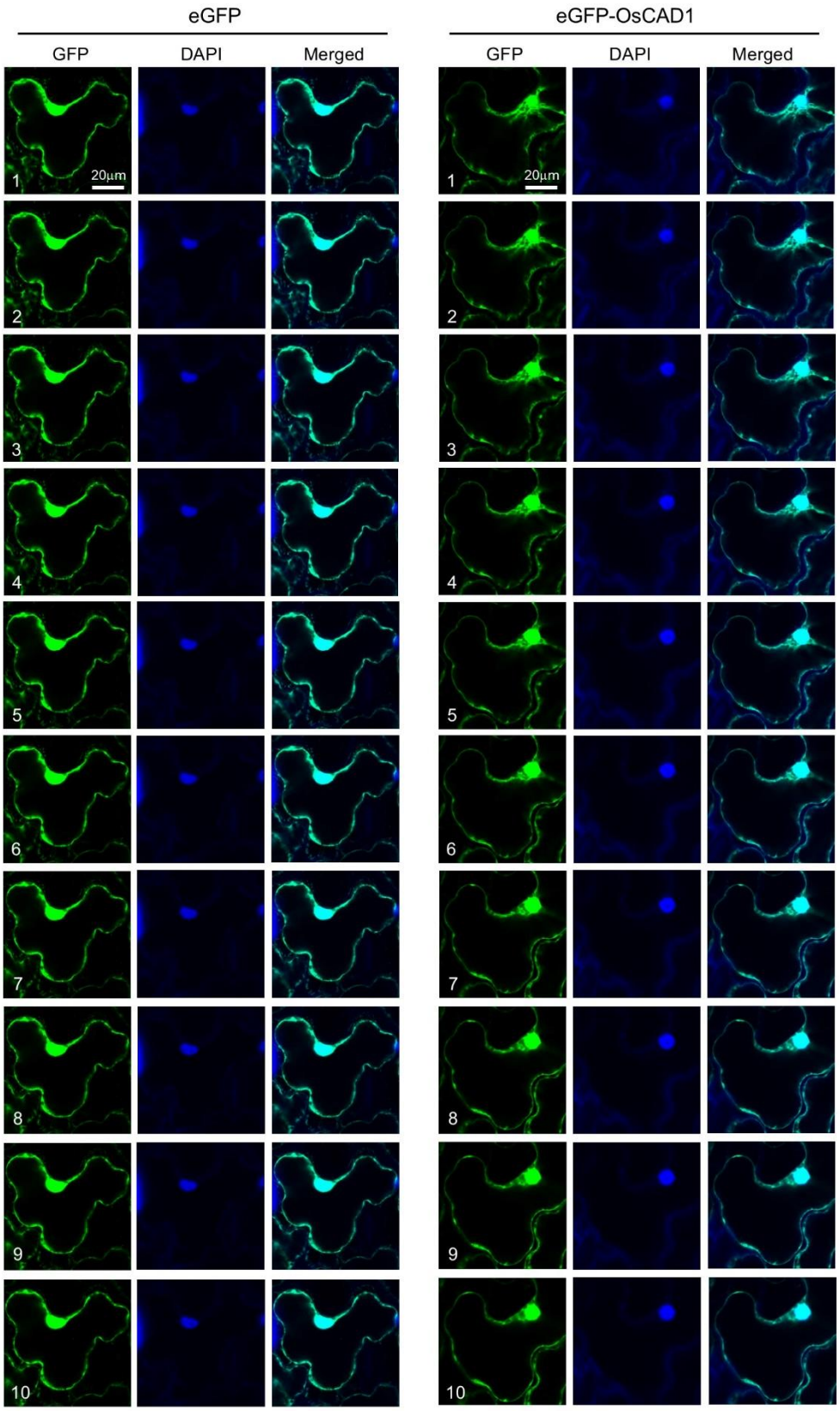

Fig. S4. Subcellular localization of eGFP and eGFP-OsCAD1 in *N. benthamiana* cells

Representative Z-stack images of *Nicotiana benthamiana* leaf cells transiently expressing eGFP (left panels) and eGFP–OsCAD1 (right panels) were acquired using confocal microscopy with a slice thickness of 1 μm.

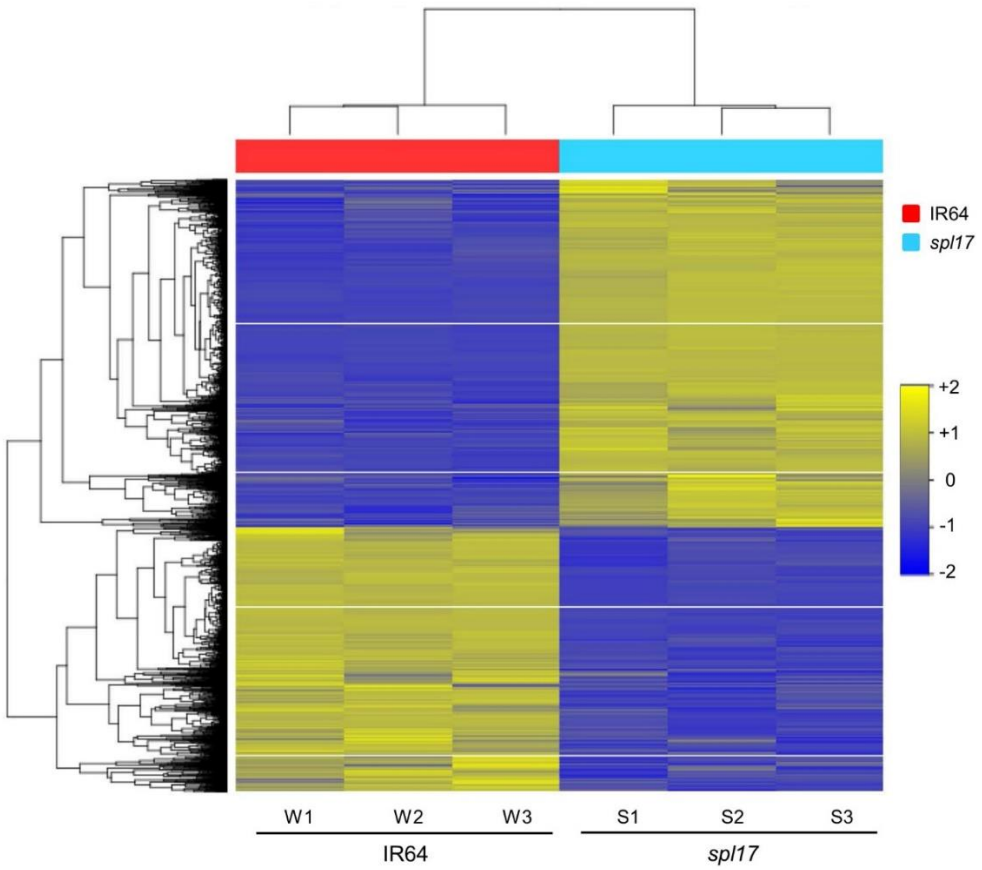

Fig. S5. Heatmap of DEGs between IR64 and *spl17*

The heatmap displays the results of hierarchical clustering analysis (Euclidean method, complete linkage). The phylogenetic tree in the left column represents the clustering of gene expression patterns from six samples. In the right column, each row corresponds to a gene, and each column represents a sample. The colour of the boxes indicates gene expression levels, with |Fold Change| ≥ 2 and raw *p*-value < 0.05. A total of 3,393 DEGs were used to construct the heatmap.

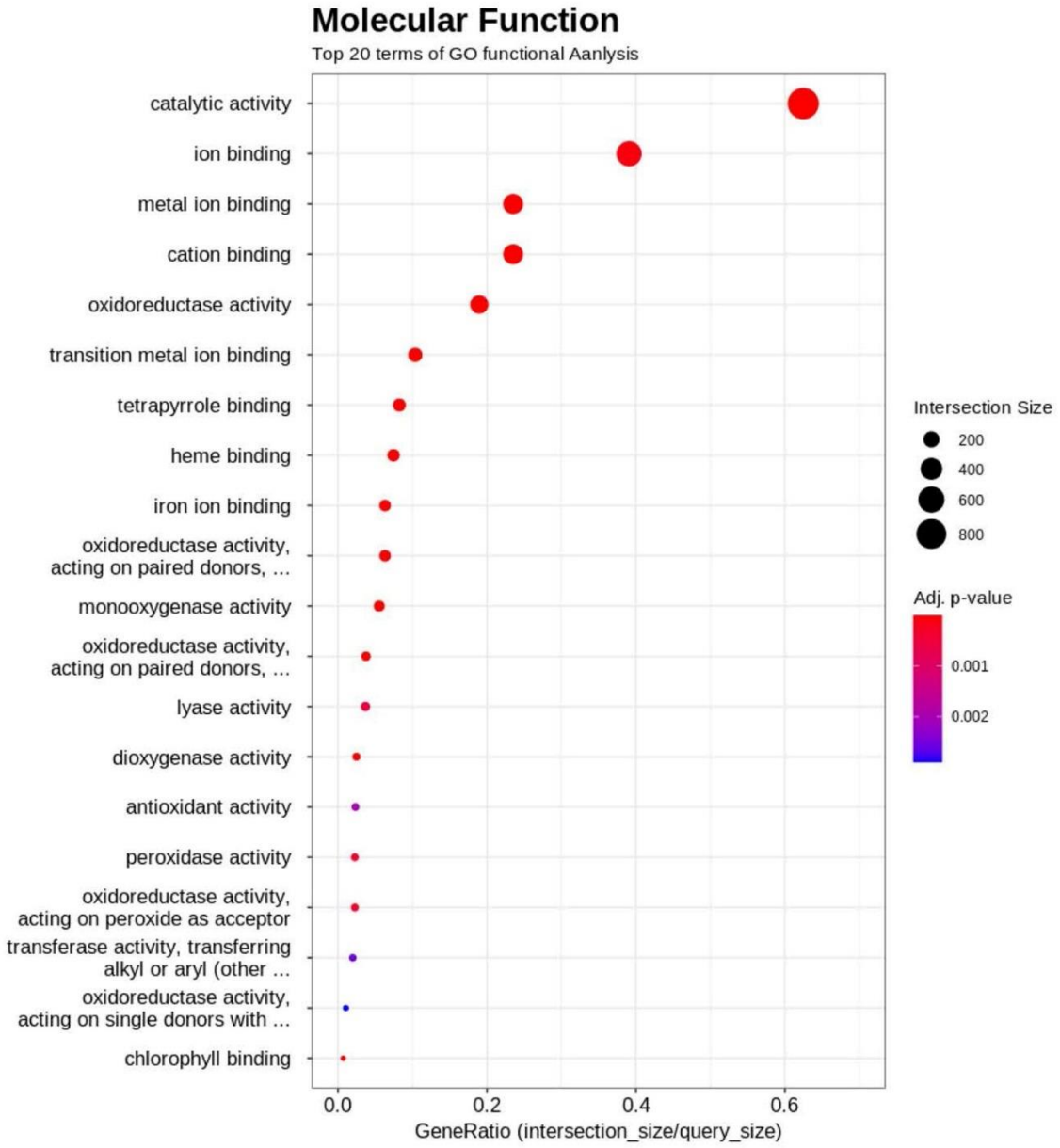

Fig. S6. Molecular function category of the DEGs through GO analysis between IR64 and *spl17*

The top 20 molecular function pathways significantly enriched in the DEGs are shown. The *x*-axis represents the gene ratio, while the *y*-axis displays the enriched molecular function pathways. The size of each circle corresponds to the number of genes, and the colour indicates the *p*-value.

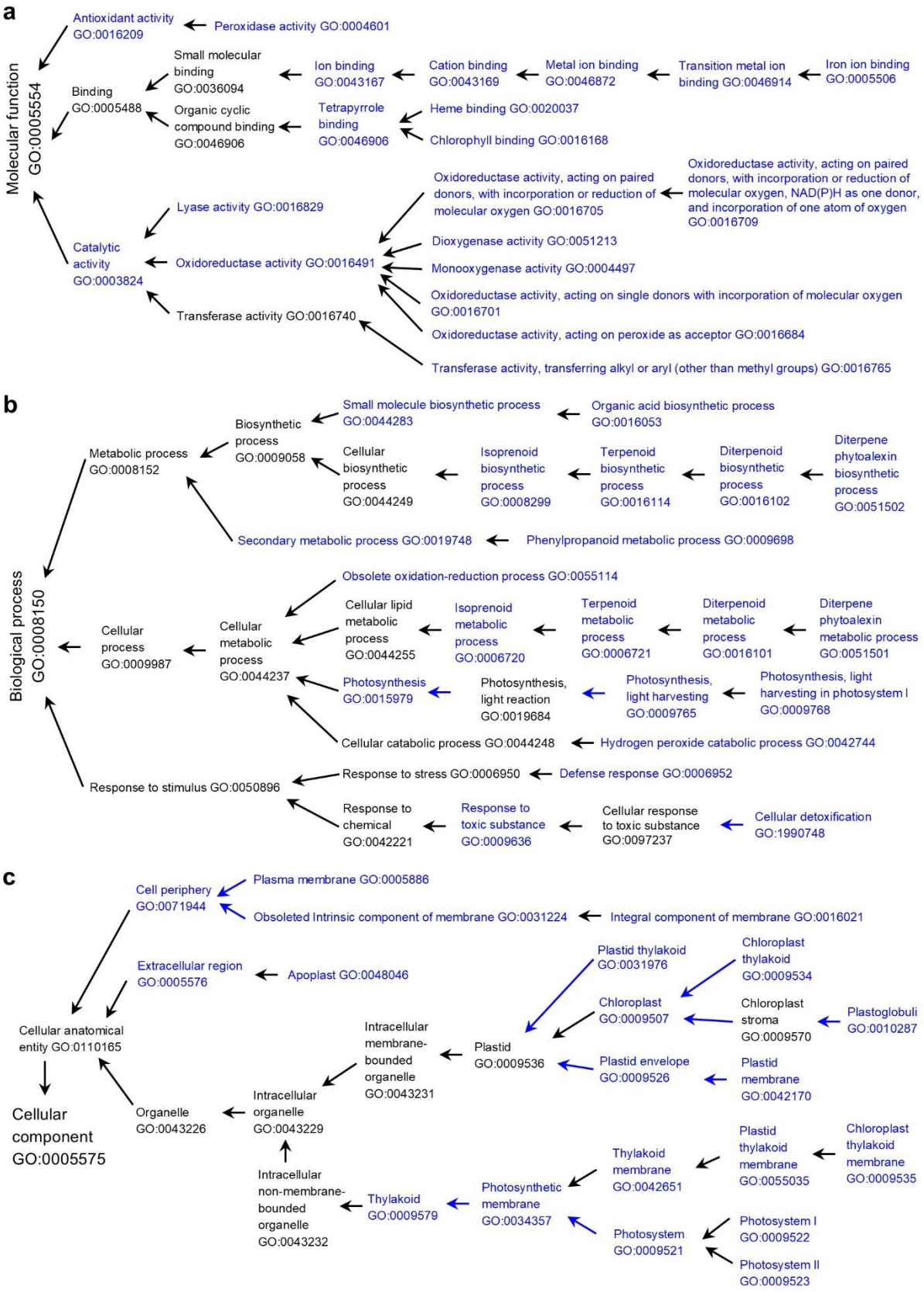

Fig. S7. Tree view of GO term enrichment analysis for DEGs between IR64 and *spl17*

(**a**) Tree view of the top 20 molecular function GO terms.

(**b**) Tree view of the top 20 biological process GO terms.

(**c**) Tree view of the top 20 cellular component GO terms.

The over-represented GO terms and their GO IDs are highlighted in blue font. Black arrows indicate hierarchical relationships, with the right GO term being a child of the left GO term. Blue arrows in (**b**) and (**c**) indicate that the right GO term is part of the left GO term.

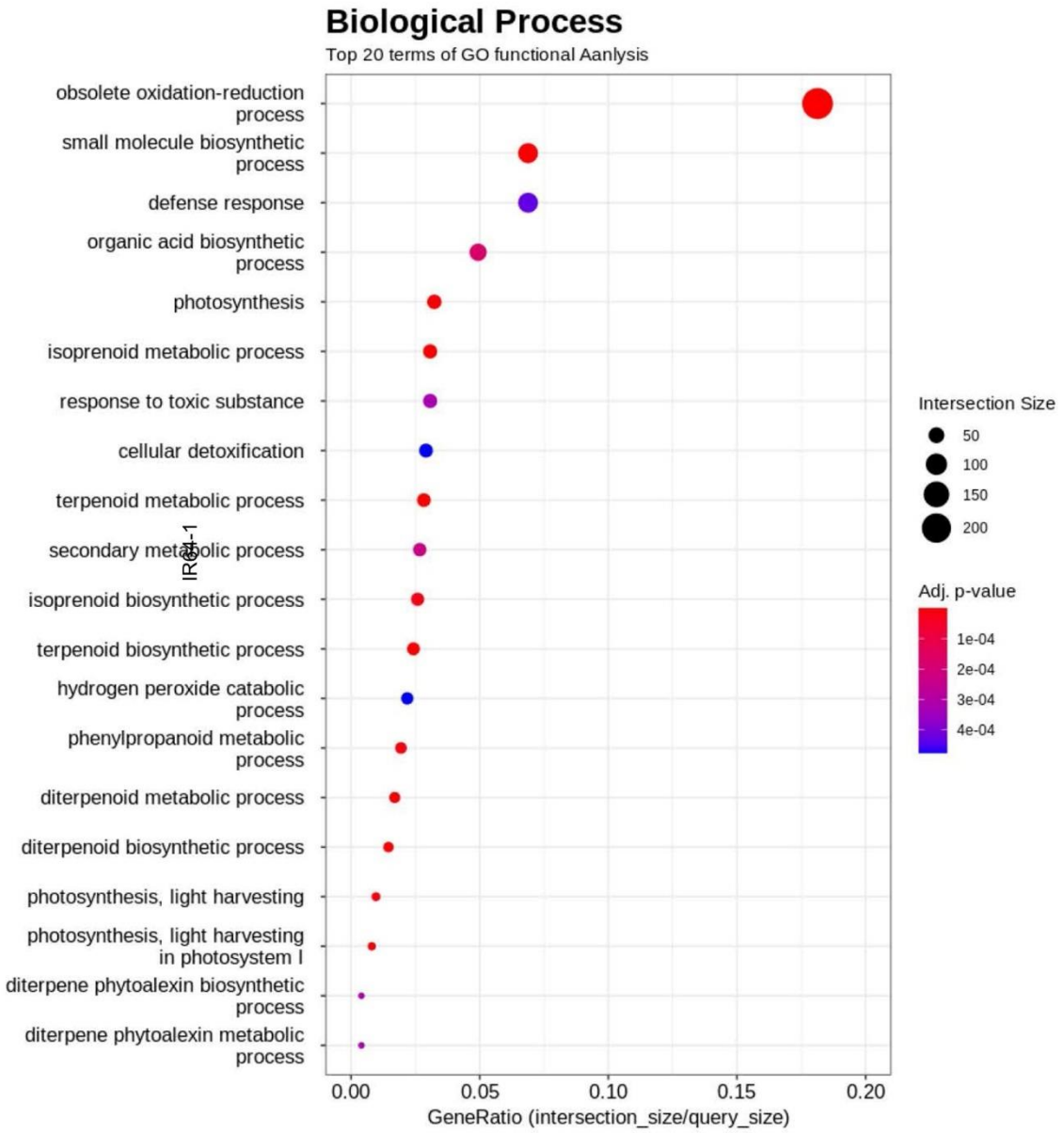

Fig. S8. Biological process category of the DEGs through GO analysis between IR64 and *spl17*
The top 20 biological processes significantly enriched in the DEGs are shown. The *x*-axis represents the gene ratio, while the *y*-axis displays the enriched biological processes. The size of each circle corresponds to the number of genes, and the colour indicates the *p*-value.

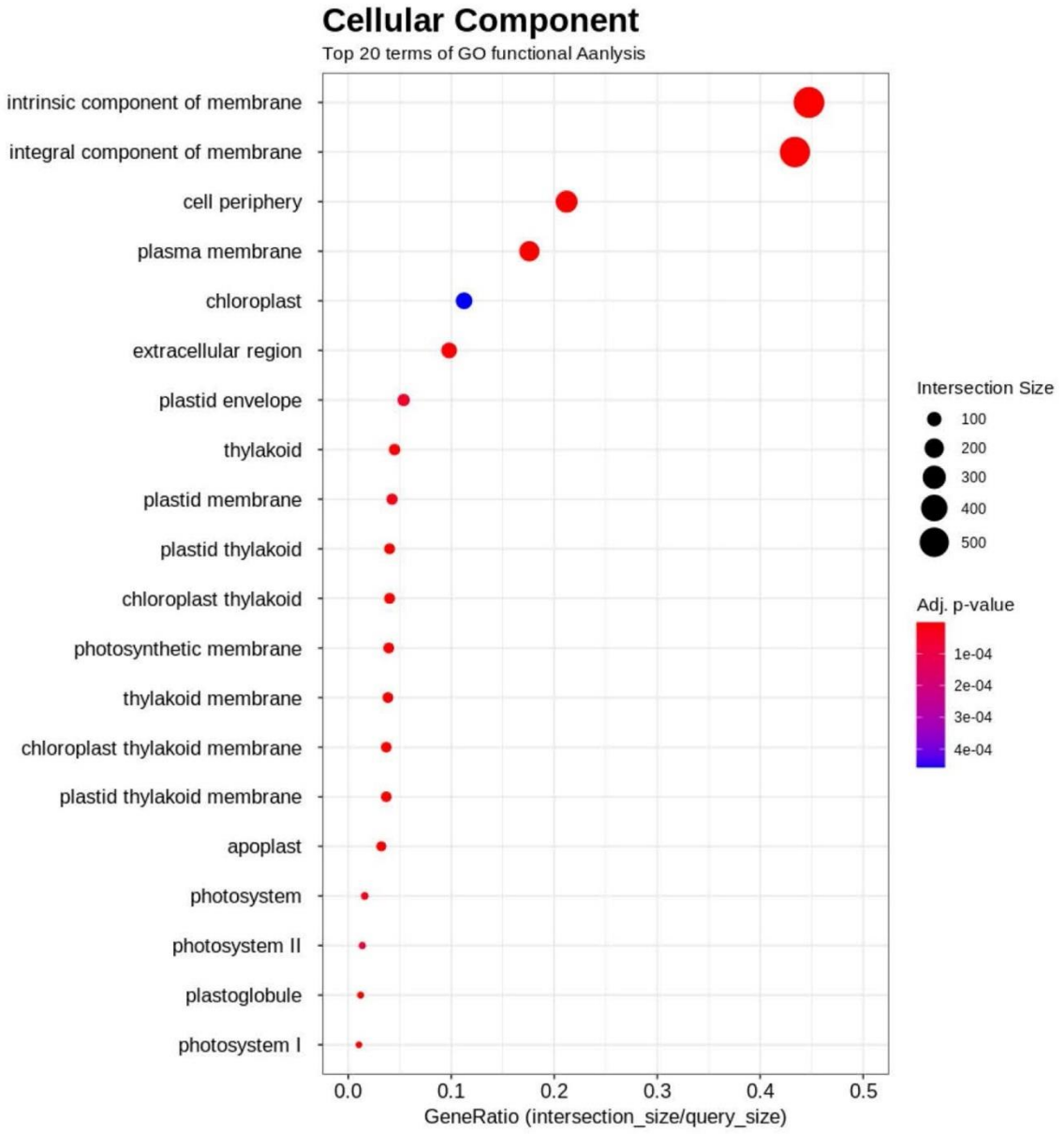

Fig. S9. Cellular component category of the DEGs through GO analysis between IR64 and *spl17* The top 20 cellular components significantly enriched in the DEGs are shown. The *x*-axis represents the gene ratio, while the y-axis displays the enriched cellular components. The size of each circle corresponds to the number of genes, and the colour indicates the *p*-value.